EFFECTS OF EXPANDING UNIVERSE IN THE SCHRÖDINGER-NEWTON APPROACH

SUBMITTED
BY

KELVIN

DIVISION OF PHYSICS & APPLIED PHYSICS
SCHOOL OF PHYSICAL AND MATHEMATICAL SCIENCES

A final year project report
presented to
Nanyang Technological University
in partial fulfilment of the
requirements for the
Bachelor of Science (Hons) in Physics / Applied Physics
Nanyang Technological University

June 2019

Final Year Project - Effects of Expanding Universe in the Schrödinger-Newton Approach

Nanyang Technological University, Singapore

Kelvin

April 16, 2019

Abstract

The cosmological constant Λ is by far the simplest and most consistent way to model the accelerating expansion of our universe. In this project, we investigate the mass and length scale in which a particle should be superposed so that the effects induced by the cosmological constant dominate the dynamics of the particle in the Schrödinger-Newton approach. Within this framework, we extend the existing Schrödinger-Newton equation by replacing the Newtonian gravitational potential with a potential that includes the effects of self-gravitating interaction and dark energy in the form of the cosmological constant. A spherically symmetric Gaussian wave function is used as our initial condition and its evolution under the "Schrödinger-Newton-Lambda equation" is solved numerically. First, we were able to recover most of the Schrödinger-Newton solutions found previously. The investigation on the mass and length scale showed terrestrial required values of approximately 10^{-20} kg superposed over the distance above 50 m. Unfortunately, the time required to observe the effects of cosmological constant for terrestrial particles turns out to be truly astronomical.

Acknowledgement

Throughout the research and writing of this thesis, I have received countless guidance and support. First and foremost, I would like to express my sincere thanks to my supervisor Professor Tomasz Paterek for his invaluable guidance and suggestions throughout the course of this project. His expertise in quantum physics has provided me with numerous insights throughout this project. I would also like to express my special gratitude to my co-supervisor Dr. Matthew James Lake whose expertise in cosmology has been instrumental in certain parts of this research. He was so supportive and willing to help me, especially in learning and understanding general relativity.

My gratitude also extends to my colleague Kelvin Onggadinata for his ideas and support, especially in verifying the numerical results using a different programming language (Python). Allow me to also thank my senior Sri Devi Wijaya who has greatly helped me in the early development of the code. The fact that this thesis is a continuation of her Final Year Project explains a lot of her role in aspiring me to explore and investigate this research topic.

Last but not least, I also say thanks with love to my family and friends who have provided me with both material and moral support throughout my studies. This thesis would not have been possible without the special contributions from the many people (mentioned explicitly or not).

Kelvin
April 16, 2019

Contents

Chapter 1

Introduction

In this chapter, we will discuss the background and motivation for this project and explain some analytical derivations involving quantum mechanics and general relativity, which will be useful in the subsequent chapters. This includes obtaining the potential from the Newtonian limit of the Einstein's field equations and the evolution of a spherically symmetric Gaussian wave function under the canonical Schrödinger equation.

1.1 Background and Motivation

According to the theory of quantum mechanics, arbitrary initial wave function has a completely deterministic time evolution. Given the Hamiltonian and the initial state, we can in principle solve the time-dependent Schrödinger equation to obtain the state at any given time. This time-evolution is a continuous and non-random process. However, a measurement process causes the wave function to collapse discontinuously into a random eigenstate of the measured observable. These two incompatible ways of state evolution prompt investigations on the possibility of their unification.

A possible unification in the context of position measurement is that gravity contributes to the collapse of the wave function. The ideas along this line have been studied by Károlyházy [1], Diósi [2], and others [3, 4]. The investigation by Diósi revolves around the uncertainty in the position of the center of mass of a macroscopic object. From classical mechanics, we know that macroscopic objects have a well-defined position at any given time. However, free particles evolving under the canonical Schrödinger equation have an increasingly larger uncertainty in the position of the center of mass. This contradiction can be resolved by conceptually forming potential wells for massive objects.

We want macroscopic objects to have deep and narrow potential wells so that their wave functions are nearly stationary. On the other hand, we require microscopic objects to have shallow and wide potential wells so that we do not change their behaviour as predicted by quantum mechanics. A logical postulate is that the size of the potential well is related to mass of the objects, and thus gravitational interaction should play a role in the process. The semiclassical approach by Møller [5] and Rosenfeld [6] is one possible way in applying gravitational interaction in quantum mechanics. In the linearized static weak-field limit, this approach results in the Schrödinger-Newton (SN) equation as proposed by Diósi [2].

The discovery of dark energy [7], an unknown form of energy causing the universe to expand in an accelerating rate, could have played a role in any model of wave function collapse induced by gravitational interaction. The Lambda Cold Dark Matter (ΛCDM) model, also known as the standard cosmological model, has the most consistent agreement with the current observational data [8]. The ΛCDM universe contains dark energy in the form of the cosmological constant. As far as we know, the effects due to the existence of dark energy in any model of wave function collapse induced by gravitational interaction has yet to be studied.

In this thesis, we aim to include the effects of dark energy in the form of the cosmological constant into the existing SN equation and study the way it affects the SN model. We will first derive a potential that includes the effects of dark enery from Einstein's field equations and use it in place of the Newtonian potential in the SN equation. We will call this modified SN equation as the Schrödinger-Newton-Lambda (SNΛ) equation from now on. The evolution of the wave functions under the SNΛ equation will be obtained numerically.

1.2 Newtonian Limit of Einstein's Field Equations

We will use the following equation, which is the semiclassical approach by Møller and Rosenfeld, as our starting point in obtaining the potential:

$$G_{\mu\nu} + \Lambda g_{\mu\nu} = \frac{8\pi\mathcal{G}}{c^4} \langle\psi| \hat{T}_{\mu\nu} |\psi\rangle \tag{1.2.1}$$

Here, $G_{\mu\nu}$ is the Einstein's tensor, $g_{\mu\nu}$ is the metric tensor, and $\mathcal{G}$ is the Newtonian gravitational constant. The energy-momentum tensor on the RHS of Einstein's field

equations is replaced with the expectation value of the energy-momentum tensor operator in the state ψ. Equation (1.2.1) can be interpreted as treating gravitational field classically while treating matter quantum mechanically. This approach causes nonlinearities in quantum mechanics as discussed by Kibble and Randjbar-Daemi [9], in the sense that the wave function depends on the metric and the metric depends on the wave function. Regardless of whether the semiclassical approach causes nonlinearities, equation (1.2.1) is too difficult to be tackled directly. We therefore, make the following assumptions, known as the Newtonian limit:

1. The gravitational field does not change significantly over time (i.e., static field). Thus, we can drop all the time derivatives of the field.

2. The sources produce weak gravitational field and hence, the metric is a nearly flat manifold. The line element for a small curvature produced by time-independent weak sources can be expressed as follows:

$$ds^2 = -\left(1 + \frac{2\Phi}{c^2}\right)(cdt)^2 + \left(1 - \frac{2\Phi}{c^2}\right)(dx^2 + dy^2 + dz^2) \tag{1.2.2}$$

   where Φ is the Newtonian gravitational potential. Thus, the metric can be expressed in the form:

$$g_{\mu\nu} = \eta_{\mu\nu} + h_{\mu\nu} \tag{1.2.3}$$

   where $\eta_{\mu\nu} = \text{diag}\,(-1, 1, 1, 1)$ is the Minkowski metric and $|h_{\mu\nu}| \ll 1$ can be thought of as small perturbations. We will treat gravity as a linearized theory by ignoring the second order and higher order terms in the perturbation.

3. The energy-momentum tensor of a matter field consisting of noninteracting incoherent matter moving with a 3D velocity $\vec{u}$ is given by

$$T^{\alpha\beta} = \rho_0 u^\alpha u^\beta = \rho \begin{pmatrix} c^2 & cu_x & cu_y & cu_z \\ cu_x & u_x u_x & u_x u_y & u_x u_z \\ cu_y & u_y u_x & u_y u_y & u_y u_z \\ cu_z & u_z u_x & u_z u_y & u_z u_z \end{pmatrix} \tag{1.2.4}$$

   where ρ_0 is the proper density. For a noninteracting matter-energy distribution that does not carry a net flow of momentum, T^{00} is much greater than T^{ij}. Thus, we will only consider the 00 component of the energy-momentum tensor.

Taking into account these assumptions (in the Newtonian limit), equation (1.2.1) reduces to the following Poisson's equation (the details of the derivation can be found in Appendix A):

$$\nabla^2\Phi(\vec{r},t) = 4\pi\mathcal{G}m|\psi(\vec{r},t)|^2 - \Lambda c^2 \tag{1.2.5}$$

This equation can be solved using the method of Green's function to give us the following solution:

$$\Phi(\vec{r},t) = -\mathcal{G}m\int\frac{|\psi(\vec{r}',t)|^2}{|\vec{r}-\vec{r}'|}d^3\vec{r}' + \frac{\Lambda c^2}{4\pi}\int\frac{1}{|\vec{r}-\vec{r}'|}d^3\vec{r}' \tag{1.2.6}$$

In this thesis, the value of the cosmological constant is taken to be [10]:

$$\Lambda = (1.36284 \pm 0.00028) \times 10^{-52}\mathrm{m}^{-2} \tag{1.2.7}$$

1.3 The Schrödinger-Newton Equation

In this thesis, we will only consider the simplest form of the SN equation: the case for a single particle with mass m. The SN equation has the form:

$$-\frac{\hbar^2}{2m}\nabla^2\psi(\vec{r},t) + m\Phi(\vec{r},t)\psi(\vec{r},t) = i\hbar\frac{\partial}{\partial t}\psi(\vec{r},t) \tag{1.3.1}$$

where $\Phi(\vec{r},t)$ is given by

$$\Phi(\vec{r},t) = -\mathcal{G}m\int\frac{|\psi(\vec{r}',t)|^2}{|\vec{r}-\vec{r}'|}d^3\vec{r}' \tag{1.3.2}$$

Substituting (1.3.2) into (1.3.1) gives us

$$-\frac{\hbar^2}{2m}\nabla^2\psi(\vec{r},t) - \mathcal{G}m^2\int\frac{|\psi(\vec{r}',t)|^2}{|\vec{r}-\vec{r}'|}d^3\vec{r}'\psi(\vec{r},t) = i\hbar\frac{\partial}{\partial t}\psi(\vec{r},t) \tag{1.3.3}$$

which is the SN equation for a single particle. The potential energy term can be thought of as a self-interacting gravitational potential by visualizing a single particle being superposed to form a mass density function $\rho(\vec{r},t) = m|\psi(\vec{r},t)|^2$ where $|\psi(\vec{r},t)|^2$ is the probability density of finding the particle at position $\vec{r}$ at a given time t.

We can also substitute (1.2.6) into (1.3.1):

$$-\frac{\hbar^2}{2m}\nabla^2\psi(\vec{r},t)+\left[-\mathcal{G}m^2\int\frac{|\psi(\vec{r}',t)|^2}{|\vec{r}-\vec{r}'|}d^3\vec{r}'+\frac{\Lambda mc^2}{4\pi}\int\frac{1}{|\vec{r}-\vec{r}'|}d^3\vec{r}'\right]\psi(\vec{r},t)=i\hbar\frac{\partial}{\partial t}\psi(\vec{r},t) \tag{1.3.4}$$

which gives us the SNΛ equation.

Both SN and SNΛ are highly nonlinear variations of the Schrödinger equation and thus, it is extremely difficult to come up with an analytical solution. Therefore, the best way to tackle this problem is by solving the equation numerically. We will explain more about the numerical method in the next chapter.

1.4 The Gaussian Function and Its Evolution under Canonical Schrödinger Equation

In general, the wave function of a free particle can be expressed in the form of a linear combination (summation) of momentum eigenfunctions (plane waves). We consider the superposition of infinitely many momentum eigenfunctions giving the Gaussian function. Physically, this means that the position of a free particle is the most localized as it could possibly be. It is not possible to have a wave function that describes a more localized free particle than the Gaussian wave function because the total uncertainty would violate the Heisenberg uncertainty principle.

It is also worth noting while momentum eigenfunctions are not normalizable (they are, however, normalized to Dirac delta function), Gaussian wave packets are normalizable to unity. This implies that for any time evolution of a Gaussian wave function, the norm of the wave function must be preserved. This is important as we want the time evolution from the numerics to preserve the norm of the wave function as well.

We will solve analytically the Schrödinger equation given the following initial wave function:

$$\psi(r,t=0)=\left(\frac{\alpha}{\pi}\right)^{3/4}e^{-\alpha r^2/2} \tag{1.4.1}$$

which is a spherically symmetric Gaussian function. The relationship between the width σ of the Gaussian function and the parameter α is given by $\sigma=\alpha^{-1/2}$. The general idea

is to first express our initial wave function (1.4.1) in terms of momentum eigenfunctions of free particle. Since we know how the eigenfunctions evolve in time, it is possible to find out how our initial wave function evolves in time.

Applying this method gives us the evolution of the initial wave function (1.4.1) which can be expressed as follows (the details of the derivation can be found in Appendix B):

$$\psi(r,t) = (\pi\alpha)^{-3/4}\left(\frac{\alpha m}{m+i\alpha\hbar t}\right)^{\frac{3}{2}}\exp\left(-\frac{\alpha m}{2(m+i\alpha\hbar t)}r^2\right) \tag{1.4.2}$$

As one would expect, the evolution retains the spherical symmetry property of the wave function. Moreover, one can check that (1.4.2) reduces to (1.4.1) when $t = 0$.

Hence, the radial probability density is given by:

$$\rho(r,t) = r^2|\psi(r,t)|^2 = r^2\,(\pi\alpha)^{-\frac{3}{2}}\left(\frac{\alpha^2 m^2}{m^2+\alpha^2\hbar^2 t^2}\right)^{\frac{3}{2}}\exp\left(-\frac{\alpha m^2}{m^2+\alpha^2\hbar^2 t^2}r^2\right) \tag{1.4.3}$$

The position where the particle is most likely to be found (i.e. the peak position of the radial probability density) is given by the point at which the first derivative of the radial probability density with respect to the radial position vanishes and reads:

$$r_p = \alpha^{-1/2}\left(1+\frac{\alpha^2\hbar^2}{m^2}t^2\right)^{\frac{1}{2}} \tag{1.4.4}$$

Equation (1.4.4) tells us that the peak radial probability density moves outward (away from the origin) over time. Furthermore, the peak is accelerating. The outward acceleration of the peak probability density can be found by taking the second derivative of r_p with respect to time:

$$\ddot{r}_p = \frac{d^2}{dt^2}\left[\alpha^{-1/2}\left(1+\frac{\alpha^2\hbar^2}{m^2}t^2\right)^{\frac{1}{2}}\right] = \frac{\hbar^2}{m^2 r_p^3} \tag{1.4.5}$$

Figure 1.1 and 1.2 show the time evolution of the radial probability density for two different masses. Based on the figures, one can conclude that the wave function spreads slower for more massive particles. This behaviour is consistent with (1.4.4) which implies that r_p is always greater for particles of smaller masses at any given time t compared to particles of greater masses.

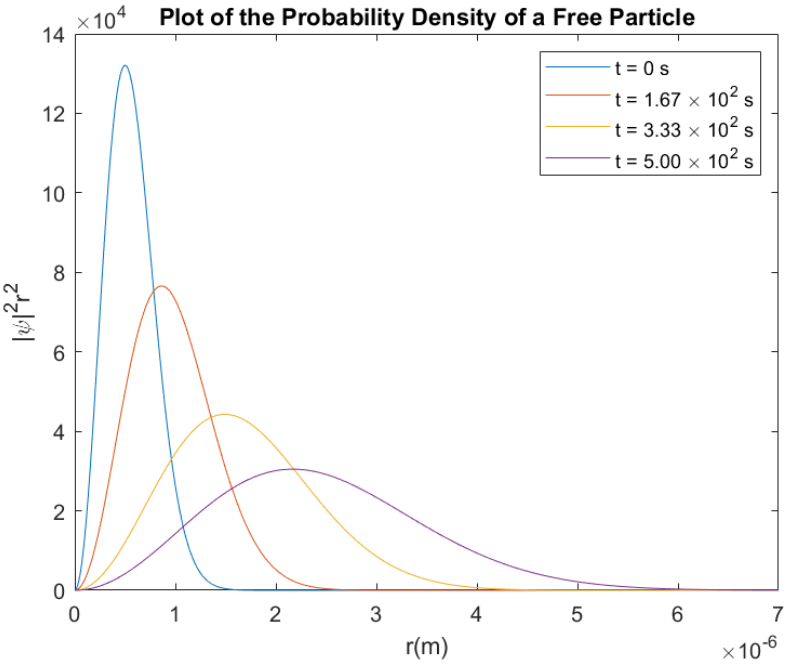

Figure 1.1: Evolution of the probability density of a free particle of mass 5×10^{-20} kg.

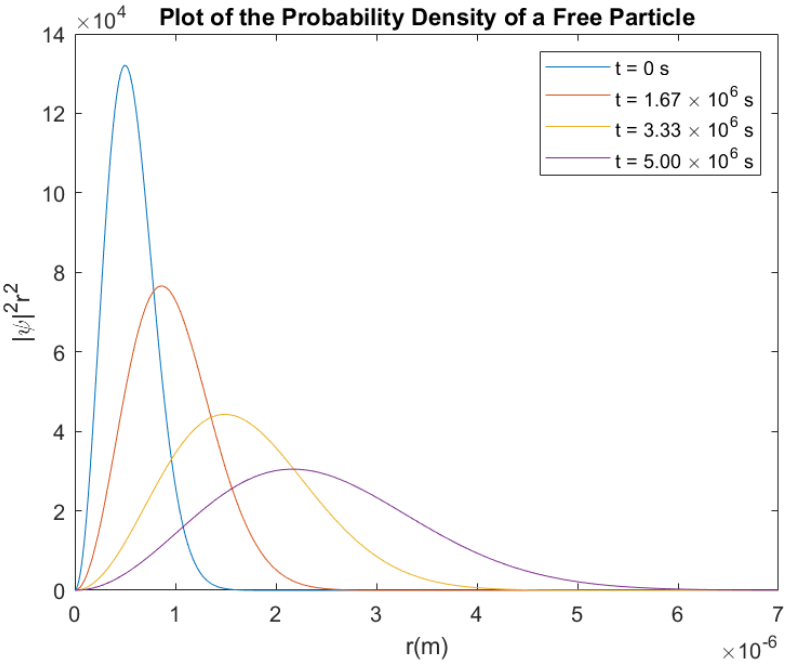

Figure 1.2: Evolution of the probability density of a free particle of mass 5×10^{-16} kg.

Solving the time evolution of our initial wave function (1.4.1) analytically is extremely important and useful since it can be used as a reference to check whether the numerics computes the time evolution accurately, at least in the case of a free particle. We can also check if the numerics for SN and SNΛ equations reduce to the free particle solution by setting the parameters of the potential so that it vanishes.

Chapter 2

Numerical Method

In this chapter, we will discuss the discretization of the SN and SNΛ equation and the numerical method used to solve them. Our method follows closely the approach used by Salzman [12]. We will also consider the problems that arose in the numerics and the conditions to obtain reliable numerical results.

2.1 Formulation of the Numerical Problem

Recall our initial wave function (1.4.1) from the previous chapter:

$$\psi(r,0) = \left(\frac{\alpha}{\pi}\right)^{3/4} e^{-\alpha r^2/2} \tag{2.1.1}$$

which only depends on the radial distance (spherically symmetric). Thus, one would expect all the evolutions of (2.1.1) to retain the spherical symmetry. Taking a spherically symmetric wave function as our initial condition greatly simplifies our problem since it allows us to treat a three-dimensional problem as a one-dimensional problem (Our problem now will only depend on the radial coordinate).

From now on, we will only consider cases with spherical symmetry. In the case of a spherically symmetric wave function, the SN equation (1.3.3) can be rewritten as follows:

$$-\frac{\hbar^2}{2m}\frac{1}{r^2}\frac{\partial}{\partial r}\left(r^2\frac{\partial\psi(r,t)}{\partial r}\right) - \mathcal{G}m^2\psi(r,t)\int\frac{|\psi(\vec{r}',t)|^2}{|\vec{r}-\vec{r}'|}d^3\vec{r}' = i\hbar\frac{\partial}{\partial t}\psi(r,t) \tag{2.1.2}$$

We can further simplify (2.1.2) by expanding the inverse distance inside the integral in terms of spherical harmonics (the details on expanding the denominator in the potential

can be found in Appendix C), which gives us:

$$-\frac{\hbar^2}{2m}\frac{1}{r^2}\frac{\partial}{\partial r}\left(r^2\frac{\partial\psi}{\partial r}\right) - 4\pi\mathcal{G}m^2\psi(r,t)\left(\frac{1}{r}\int_0^r |\psi(r',t)|^2 r'^2 dr' + \int_r^\infty |\psi(r',t)|^2 r' dr'\right) = i\hbar\frac{\partial\psi}{\partial t} \tag{2.1.3}$$

By the similar method, the SNΛ equation can also be rewritten as follows:

$$-\frac{\hbar^2}{2m}\frac{1}{r^2}\frac{\partial}{\partial r}\left(r^2\frac{\partial\psi}{\partial r}\right) - 4\pi\mathcal{G}m^2\psi(r,t)\left(\frac{1}{r}\int_0^r |\psi(r',t)|^2 r'^2 dr' + \int_r^\infty |\psi(r',t)|^2 r' dr'\right) + \Lambda mc^2\psi(r,t)\left(\frac{1}{r}\int_0^r r'^2 dr' + \int_r^\infty r' dr'\right) = i\hbar\frac{\partial\psi}{\partial t} \tag{2.1.4}$$

Thus, we will solve (2.1.3) and (2.1.4) numerically given the initial wave function (2.1.1).

2.2 Coordinate Singularity: Laplacian at the Spherical Polar Origin

Equation (2.1.3) and (2.1.4) contain a problematic term for our numerics, namely the Laplacian of the wave function at the origin. In spherical polar coordinates, the Laplacian of the spherically symmetric wave function is given by:

$$\nabla_r^2\psi = \frac{1}{r^2}\frac{\partial}{\partial r}\left(r^2\frac{\partial\psi}{\partial r}\right) = \frac{\partial^2\psi}{\partial r^2} + \frac{2}{r}\frac{\partial\psi}{\partial r}. \tag{2.2.1}$$

which is not well-defined at $r = 0$. We will use one of the arguments provided by Salzman [12] to tackle this problem. The idea is to Taylor expand the first derivative about $r = 0$ in (2.2.1) and take its limit as r approaches zero. Mathematically, we can write

$$\lim_{r\to 0}\frac{2}{r}\frac{\partial\psi}{\partial r} = \lim_{r\to 0}\frac{2}{r}\left(\left.\frac{\partial\psi}{\partial r}\right|_{r=0} + r\left.\frac{\partial^2\psi}{\partial r^2}\right|_{r=0} + \frac{r^2}{2}\left.\frac{\partial^3\psi}{\partial r^3}\right|_{r=0} + \cdots\right) \tag{2.2.2}$$

Notice that in the case of spherical symmetry, the Hamiltonian for the SN and SNΛ equation commute with the parity operator. Thus, time evolutions must conserve parity. Our initial wave function (the Gaussian function) is an even function. Since parity is conserved, its time evolution must be an even function as well, i.e., $\psi(r,t) = \psi(-r,t)$.

We know that the first derivative of an even function is an odd function. Thus,

$$\lim_{r\to 0}\frac{\partial\psi(r,t)}{\partial r}=0 \tag{2.2.3}$$

With this in mind, equation (2.2.2) becomes:

$$\lim_{r\to 0}\frac{2}{r}\frac{\partial\psi}{\partial r}=2\frac{\partial^2\psi}{\partial r^2} \tag{2.2.4}$$

and finally we have:

$$\nabla_r^2\psi=\frac{1}{r^2}\frac{\partial}{\partial r}\left(r^2\frac{\partial\psi}{\partial r}\right)=3\frac{\partial^2\psi}{\partial r^2}\qquad\text{for}\qquad r=0. \tag{2.2.5}$$

In view of (2.2.3), we can also use L'Hôpital's rule to solve:

$$\lim_{r\to 0}\frac{2}{r}\frac{\partial\psi}{\partial r}=2\lim_{r\to 0}\frac{\frac{\partial\psi}{\partial r}}{r}=2\frac{\partial^2\psi}{\partial r^2} \tag{2.2.6}$$

which is in complete agreement with (2.2.4).

2.3 Discretization of the Time-Dependent Schrödinger Equation

To solve the Schrödinger equation numerically, we must first discretize the domain of our problem: space and time. In this way, the solution to the Schrödinger equation can be written in the form of a two-dimensional matrix with each matrix element ψ_j^n representing the solution at a distance of $j\Delta r$ from the origin and at a time of $n\Delta t$, i.e., $\psi_j^n=\psi(j\Delta r,n\Delta t)$.

2.3.1 Problems with Explicit and Implicit Form of Discretization

The general solution to the time-dependent Schrödinger equation is given by:

$$\psi(r,t+\Delta t)=e^{-i\hat{H}\Delta t/\hbar}\psi(r,t) \tag{2.3.1}$$

In a discretized form, (2.3.1) becomes:

$$\psi_j^{n+1}=e^{-i\hat{H}\Delta t/\hbar}\psi_j^n \tag{2.3.2}$$

We will now perform Taylor series expansion on the exponential function keeping up to first order term in Δt:

$$\psi_j^{n+1} \approx \left(\hat{\mathbb{1}} - \frac{i\hat{H}\Delta t}{\hbar}\right)\psi_j^n \tag{2.3.3}$$

This form of discretization is known as the explicit Forward Time Centered Space (FTCS) discretization. However, this strategy turns out to be unconditionally unstable based on Von Neumann's analysis [14, see pg. 836 and 837]. This means that any small errors will incrementally get worse for each timestep which can eventually disrupt the whole numerical results. Moreover, equation (2.3.3) is not unitary and thus, it does not preserve the norm of the wavefunction.

Another method is to translate the wave function backward in time, i.e.,

$$e^{+i\hat{H}\Delta t/\hbar}\psi(r, t + \Delta t) = \psi(r, t) \tag{2.3.4}$$

Performing Taylor series expansion and writing (2.3.4) in a discretized form, we have:

$$\psi_j^{n+1} \approx \left(\hat{\mathbb{1}} + \frac{i\hat{H}\Delta t}{\hbar}\right)^{-1}\psi_j^n \tag{2.3.5}$$

which is also known as the implicit form. Once again, equation (2.3.5) does not preserve the norm of the wave function although this method is likely to be stable based on Von Neumann's analysis [14, see pg. 849 and 852].

2.3.2 Cayley's Form

The general idea of Cayley's form [14, see pg. 853] is to translate the wave function at timestep $n + 1$ backward in time by $\Delta t/2$ and translate the wave function at timestep n forward in time by $\Delta t/2$ as well. Since the time evolution is a continuous process, we require both translated wave functions to be equal at the middle of the timestep. Mathematically, we can write:

$$e^{+i\hat{H}\Delta t/2\hbar}\psi(r, t + \Delta t) = e^{-i\hat{H}\Delta t/2\hbar}\psi(r, t) \tag{2.3.6}$$

Performing Taylor series expansion and writing (2.3.6) in the discretized form, we have:

$$\psi_j^{n+1} \approx \left(\hat{\mathbb{1}} + \frac{i\hat{H}\Delta t}{2\hbar}\right)^{-1}\left(\hat{\mathbb{1}} - \frac{i\hat{H}\Delta t}{2\hbar}\right)\psi_j^n = \left[2\left(\hat{\mathbb{1}} + \frac{i\Delta t}{2\hbar}\hat{H}\right)^{-1} - \hat{\mathbb{1}}\right]\psi_j^n \tag{2.3.7}$$

which is unitary and thus, preserves the norm of the wave function. Let us denote:

$$\hat{Q}^{-1} = 2\left(\hat{\mathbb{1}} + \frac{i\Delta t}{2\hbar}\hat{H}\right)^{-1} \qquad \text{and} \qquad \hat{Q} = \frac{1}{2}\left(\hat{\mathbb{1}} + \frac{i\Delta t}{2\hbar}\hat{H}\right) \tag{2.3.8}$$

Thus, (2.3.7) becomes:

$$\psi^{n+1} = \hat{Q}^{-1}\psi^n - \psi^n = \chi^n - \psi^n \tag{2.3.9}$$

The next step is to solve for χ^n given ψ^n. To do this, we need the explicit expression for $\hat{Q}$.

2.3.3 The Difference Equations

We will now find the expression for $\hat{Q}$ by substituting the Hamiltonian into (2.3.8):

$$\hat{Q} = \frac{1}{2}\left[\hat{\mathbb{1}} + \frac{i\Delta t}{2\hbar}\left(-\frac{\hbar^2}{2m}\nabla^2 + \hat{V}\right)\right] \tag{2.3.10}$$

Recall that the Laplacian at the origin must be treated differently according to (2.2.5). Thus, (2.3.10) can be rewritten as follows:

$$\hat{Q} = \begin{cases} \dfrac{1}{2}\left[\hat{\mathbb{1}} + \dfrac{i\Delta t}{2\hbar}V_j^n - \dfrac{3i\hbar\Delta t}{4m}\dfrac{\partial^2}{\partial r^2}\right] & \text{for} \quad r = 0 \\ \dfrac{1}{2}\left[\hat{\mathbb{1}} + \dfrac{i\Delta t}{2\hbar}V_j^n - \dfrac{i\hbar\Delta t}{4m}\dfrac{1}{r^2}\dfrac{\partial}{\partial r}\left(r^2\dfrac{\partial}{\partial r}\right)\right] & \text{for} \quad r \neq 0 \end{cases} \tag{2.3.11}$$

In solving the linear equations $\hat{Q}\chi_j^n = \psi_j^n$, we need to act the operator $\hat{Q}$ on χ_j^n. It is already obvious that $\hat{Q}\chi_j^n$ has to be treated differently at the spatial origin. Besides, we also require the wave function to vanish at the spatial endpoint (numerical infinity). Therefore, we have to consider 3 different cases:

1. Case 1: For $j \neq 0, N-1$

$$\begin{aligned}
\hat{Q}\chi_j^n &= \frac{1}{2}\left[\hat{\mathbb{1}} + \frac{i\Delta t}{2\hbar}V_j^n\right]\chi_j^n - \frac{i\hbar\Delta t}{4m}\left[\frac{1}{2}\frac{\partial^2\chi_j^n}{\partial r^2} + \frac{1}{r}\frac{\partial\chi_j^n}{\partial r}\right] \\
&\approx \frac{1}{2}\left[\hat{\mathbb{1}} + \frac{i\Delta t}{2\hbar}V_j^n\right]\chi_j^n - \frac{i\hbar\Delta t}{4m}\left[\frac{1}{2}\left(\frac{\chi_{j+1}^n - 2\chi_j^n + \chi_{j-1}^n}{(\Delta r)^2}\right) + \frac{1}{j\Delta r}\left(\frac{\chi_{j+1}^n - \chi_{j-1}^n}{2\Delta r}\right)\right] \\
&= -\frac{i\hbar\Delta t}{8m(\Delta r)^2}\left(\frac{j-1}{j}\right)\chi_{j-1}^n + \frac{1}{2}\left[1 + \frac{i\Delta t}{2\hbar}V_j^n + \frac{i\hbar\Delta t}{4m(\Delta r)^2}\right]\chi_j^n - \frac{i\hbar\Delta t}{8m(\Delta r)^2}\left(\frac{j+1}{j}\right)\chi_{j+1}^n
\end{aligned}$$

Let us denote:

$$K = \frac{i\hbar}{8m} \qquad R = \frac{\Delta t}{(\Delta r)^2} \qquad P = \frac{i\Delta t}{2\hbar} \tag{2.3.12}$$

Thus, we have:

$$\hat{Q}\chi_j^n = -KR\left(\frac{j-1}{j}\right)\chi_{j-1}^n + \frac{1}{2}\left[1 + PV_j^n + 2KR\right]\chi_j^n - KR\left(\frac{j+1}{j}\right)\chi_{j+1}^n \tag{2.3.13}$$

2. Case 2: For $j = N-1$

In this case, $\psi_N^n = 0$ which implies that $\chi_N^n = 0$ as well. Therefore, from (2.3.13), we have:

$$\hat{Q}\chi_{N-1}^n = -KR\left(\frac{N-2}{N-1}\right)\chi_{N-2}^n + \frac{1}{2}\left[1 + PV_{N-1}^n + 2KR\right]\chi_{N-1}^n \tag{2.3.14}$$

3. Case 3: For $j = 0$

$$\begin{aligned}
\hat{Q}\chi_j^n &\approx \frac{1}{2}\left[\hat{\mathbb{1}} + \frac{i\Delta t}{2\hbar}V_j^n\right]\chi_j^n - \frac{3i\hbar\Delta t}{4m}\left(\frac{\chi_{j+1}^n - 2\chi_j^n + \chi_{j-1}^n}{(\Delta r)^2}\right) \\
&= -\frac{3i\hbar\Delta t}{8m(\Delta r)^2}\chi_{j-1}^n + \frac{1}{2}\left[1 + \frac{i\Delta t}{2\hbar}V_j^n + \frac{3i\hbar\Delta t}{2m(\Delta r)^2}\right]\chi_j^n - \frac{3i\hbar\Delta t}{8m(\Delta r)^2}\chi_{j+1}^n
\end{aligned}$$

Applying the constants defined by (2.3.13) and taking into account the fact that $\chi_{-1}^n = \chi_1^n$ due to spherical symmetry, we have:

$$\hat{Q}\chi_0^n = \frac{1}{2}\left[1 + PV_0^n + 12KR\right]\chi_0^n - 6KR\chi_1^n \tag{2.3.15}$$

The linear equations $\hat{Q}\chi_j^n = \psi_j^n$ can be written in the following matrix form:

$$\begin{pmatrix} b_0 & c_0 & & & & & & \\ a_1 & b_1 & c_1 & & & & & \\ & a_2 & b_2 & c_2 & & & & \\ & & & \ddots & & & & \\ & & & & a_{N-2} & b_{N-2} & c_{N-2} \\ & & & & & a_{N-1} & b_{N-1} \end{pmatrix} \begin{pmatrix} \chi_0 \\ \chi_1 \\ \chi_2 \\ \vdots \\ \chi_{N-2} \\ \chi_{N-1} \end{pmatrix} = \begin{pmatrix} \psi_0 \\ \psi_1 \\ \psi_2 \\ \vdots \\ \psi_{N-2} \\ \psi_{N-1} \end{pmatrix} \tag{2.3.16}$$

Here, $\hat{Q}$ is represented by the tridiagonal matrix. The matrix elements: a_i denotes the superdiagonal elements, b_i denotes the diagonal elements, and c_i denotes the subdiagonal elements. The next step is to solve (2.3.16) using Thomas Algorithm.

2.3.4 Solving the Tridiagonal Systems of Linear Equations: Thomas Algorithm

Performing the matrix multiplication on the LHS of (2.3.16) gives the following set of linear equations:

$$\begin{pmatrix} b_0\chi_0 + c_0\chi_1 \\ a_1\chi_0 + b_1\chi_1 + c_1\chi_2 \\ a_2\chi_1 + b_2\chi_2 + c_2\chi_3 \\ \vdots \\ a_{N-2}\chi_{N-3} + b_{N-2}\chi_{N-2} + c_{N-2}\chi_{N-1} \\ a_{N-1}\chi_{N-2} + b_{N-1}\chi_{N-1} \end{pmatrix} = \begin{pmatrix} \psi_0 \\ \psi_1 \\ \psi_2 \\ \vdots \\ \psi_{N-2} \\ \psi_{N-1} \end{pmatrix} \tag{2.3.17}$$

Our goal is to eliminate a_i. We first eliminate a_1 by multiplying the zeroth linear equation with a_1/b_0 (recall that $b_0 \neq 0$) and subtracting it from the first equation, which gives:

$$\left(b_1 - \frac{a_1}{b_0}c_0\right)\chi_1 + c_1\chi_2 = \psi_1 - \frac{a_1}{b_0}\psi_0 \tag{2.3.18}$$

Let $b_0 = B_0$, $\psi_0 = D_0$, and define:

$$B_1 = b_1 - \frac{a_1}{B_0}c_0 \qquad \text{and} \qquad D_1 = \psi_1 - \frac{a_1}{B_0}\psi_0 \tag{2.3.19}$$

Thus, we can rewrite (2.3.17) as follows:

$$\begin{pmatrix} B_0\chi_0 + c_0\chi_1 \\ B_1\chi_1 + c_1\chi_2 \\ a_2\chi_1 + b_2\chi_2 + c_2\chi_3 \\ \vdots \\ a_{N-2}\chi_{N-3} + b_{N-2}\chi_{N-2} + c_{N-2}\chi_{N-1} \\ a_{N-1}\chi_{N-2} + b_{N-1}\chi_{N-1} \end{pmatrix} = \begin{pmatrix} D_0 \\ D_1 \\ \psi_2 \\ \vdots \\ \psi_{N-2} \\ \psi_{N-1} \end{pmatrix} \tag{2.3.20}$$

We repeat the same procedure to eliminate a_2. Multiplying the first linear equation with a_2/B_1 and subtracting it from the second equation gives:

$$\left(b_2 - \frac{a_2}{B_1}c_1\right)\chi_2 + c_2\chi_3 = \psi_2 - \frac{a_2}{B_1}D_1 \tag{2.3.21}$$

Again, we define:

$$B_2 = b_2 - \frac{a_2}{B_1}c_1 \qquad \text{and} \qquad D_2 = \psi_2 - \frac{a_2}{B_1}D_1 \tag{2.3.22}$$

This procedure is repeated up to the last linear equation, which gives the following set of linear equations:

$$\begin{pmatrix} B_0\chi_0 + c_0\chi_1 \\ B_1\chi_1 + c_1\chi_2 \\ B_2\chi_2 + c_2\chi_3 \\ \vdots \\ B_{N-2}\chi_{N-2} + c_{N-2}\chi_{N-1} \\ B_{N-1}\chi_{N-1} \end{pmatrix} = \begin{pmatrix} D_0 \\ D_1 \\ D_2 \\ \vdots \\ D_{N-2} \\ D_{N-1} \end{pmatrix} \tag{2.3.23}$$

where

$$B_i = b_i - \frac{a_i}{B_{i-1}}c_{i-1}, \quad D_i = \psi_i - \frac{a_i}{B_{i-1}}D_{i-1} \quad \text{for} \quad i = 1, 2, \cdots, N-1. \tag{2.3.24}$$

The last linear equation in (2.3.23) allows us to solve for χ_{N-1}. With χ_{N-1}, we can work backwards and solve for χ_{N-2} and so on. As seen, the Thomas Algorithm is an extremely efficient way to solve tridiagonal systems of linear equations since it allows us to work with and store data in one-dimensional vectors instead of a two-dimensional matrix.

2.4 Discretization of the Potential for Schrödinger-Newton-Lambda (SNΛ) Equation

The potential of the SNΛ equation in the case of spherical symmetry is given by:

$$\Phi(r,t) = -4\pi\mathcal{G}m\left(\frac{1}{r}\int_0^r |\psi(r',t)|^2 r'^2 dr' + \int_r^\infty |\psi(r',t)|^2 r' dr'\right) + \Lambda c^2\left(\frac{1}{r}\int_0^r r'^2 dr' + \int_r^\infty r' dr'\right) \tag{2.4.1}$$

and the potential of the SN equation can be obtained by substituting $\Lambda = 0$ into (2.4.1). In a discretized form, (2.4.1) becomes:

$$V_j^n = -4\pi\mathcal{G}m\left(\frac{1}{j(\Delta r)}\sum_{i=0}^{j-1}|\psi_i^n|^2(i\Delta r)^2\Delta r + \sum_{i=j}^{N-1}|\psi_i^n|^2(i\Delta r)\Delta r\right) + \Lambda c^2\left(\frac{1}{j(\Delta r)}\sum_{i=0}^{j-1}(i\Delta r)^2\Delta r + \sum_{i=j}^{N-1}(i\Delta r)\Delta r\right)$$
$$V_j^n = -4\pi\mathcal{G}m(\Delta r)^2\left(\frac{1}{j}\sum_{i=0}^{j-1}|\psi_i^n|^2 i^2 + \sum_{i=j}^{N-1}|\psi_i^n|^2 i\right) + \Lambda c^2(\Delta r)^2\left(\frac{1}{j}\sum_{i=0}^{j-1} i^2 + \sum_{i=j}^{N-1} i\right) \tag{2.4.2}$$

2.5 Conditions for Valid Numerics

Recall that in solving the Schrödinger equation numerically, we used the Cayley's form of discretization which always preserves the norm of the wave function. This together with our initial wave function, which is normalized, implies that the wave function at any given time must vanish as the radial distance r goes to infinity, i.e., $\psi(r \to \infty, t) = 0$. However, in deriving the difference equations, we have imposed this boundary condition at the numerical infinity (which is not the true infinity). This is problematic since analytically, the wave function at a given time is not necessarily zero at the numerical infinity.

As illustrated in Figure 2.1, imposing this boundary condition at the numerical infinity causes any wave function which is non-zero at the numerical infinity to experience a "reflection" by the numerical infinity.

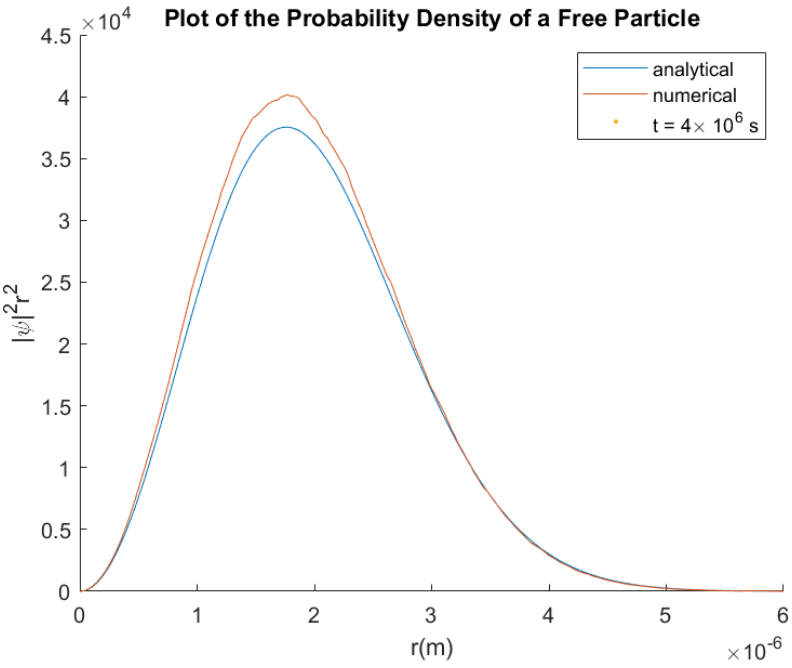
Plot of the Probability Density of a Free Particle
×10^4
4.5
4
3.5
3
2.5
2
1.5
1
0.5
0
|ψ|^2_r^2
analytical
numerical
t = 4× 10^6 s
0
1
2
3
4
5
6
r(m)
×10^-6

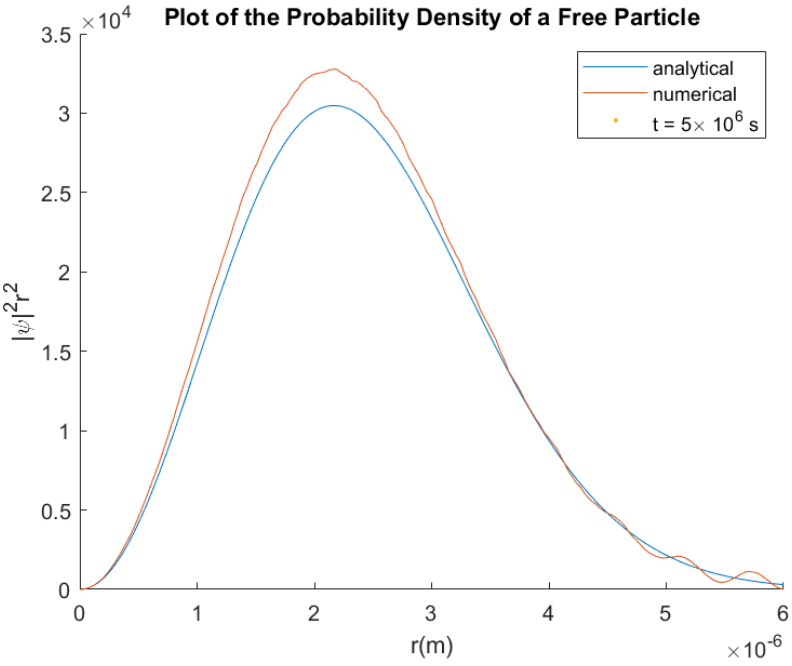
Plot of the Probability Density of a Free Particle
×10^4
3.5
3
2.5
2
1.5
1
0.5
0
|ψ|^2_r^2
analytical
numerical
t = 5× 10^6 s
0
1
2
3
4
5
6
r(m)
×10^-6

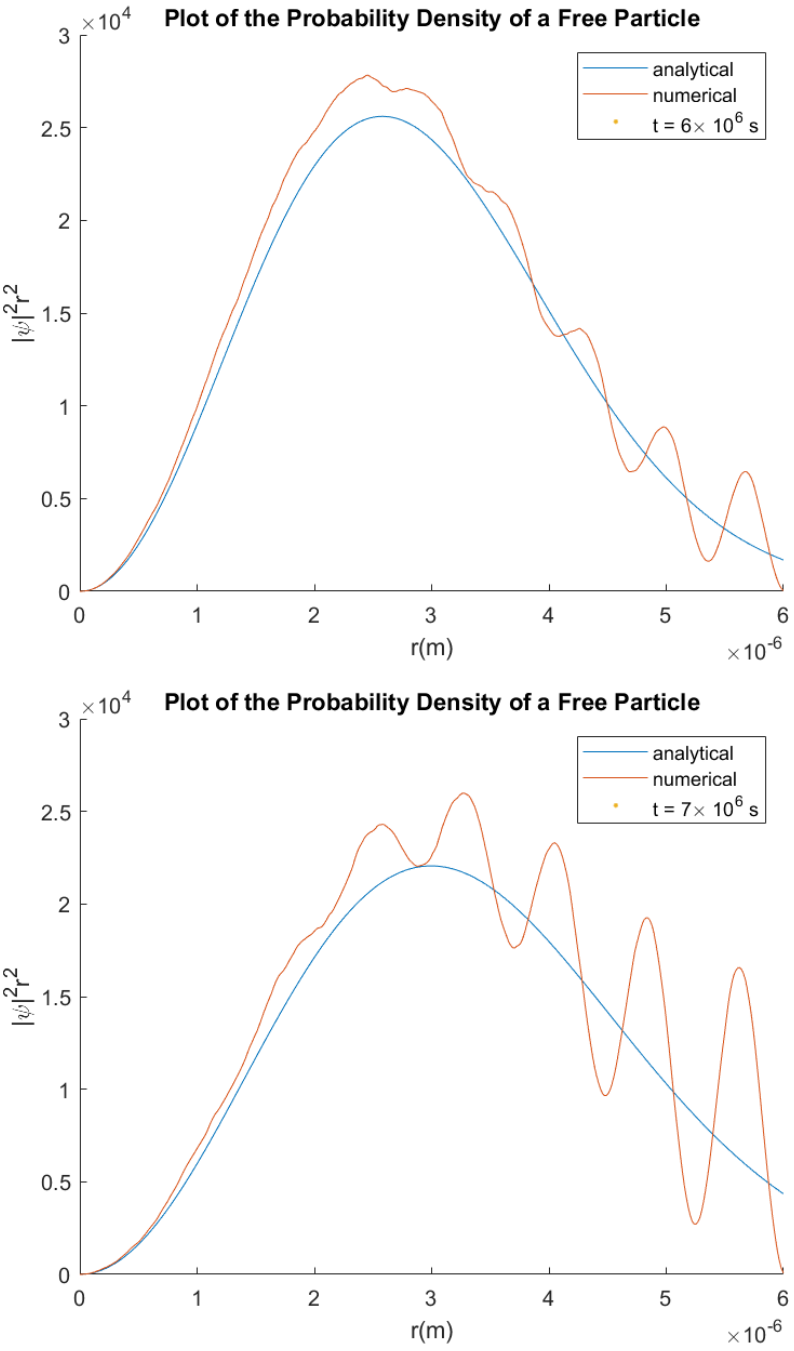

Figure 2.1: Reflection of the wave function ($m = 5 \times 10^{-16}$ kg) for different times.

As far as one can see, this "reflection" causes the numerical results to be invalid. A possible way to obtain accurate solutions from the numerics is to set a time range in

which the effects due to reflection are negligible. The disadvantage of this approach is that the dynamics beyond the time range can not be observed.

After fixing a time range such that the effects due to reflection is negligible, one must also take into consideration the number of discrete points in space and time used in the numerics. In order to obtain valid numerical results, the number of time steps has to be much larger compared to the number of position "steps". However, we do not want the number of spatial points to be too low in order to obtain a smooth curve.

Chapter 3

Numerical Review Using Schrödinger Equation

In this chapter, we will solve the canonical Schrödinger equation with different potentials (zero and step potential) numerically and see if the results obtained coincide with our understanding of quantum mechanics. This mainly serves as a method to check if the numerics is valid, at least in the case of the canonical Schrödinger equation.

3.1 The Free Particle

As explained in section 1.4, the radial probability density of a free particle described by a Gaussian wave function spreads over time. We will solve the evolution of our initial wave function numerically and plot the time evolution of the radial probability density. In the case of a free particle, the potential is set to zero at all times and at all points in space, i.e., $V_j^n = 0$ for all j and n.

Figure 3.1 shows the comparison between the evolution of the radial probability density obtained numerically and analytically. As can be seen, the numerical results are in good agreement with our analytical predictions. The height of the analytical Gaussian peak is slightly lower compared to the numerical Gaussian peak. This is as expected since probability is allowed to "leak out" beyond the numerical infinity in the analytical case but not allowed in the numerical case. Since it is always possible to compare the numerical to the analytical results in the case of a free particle, the numerics for the free particle acts as a platform to fine-tune the parameters, such as the time range and number of steps, as the numerics is used to solve for the SN and SNΛ equation.

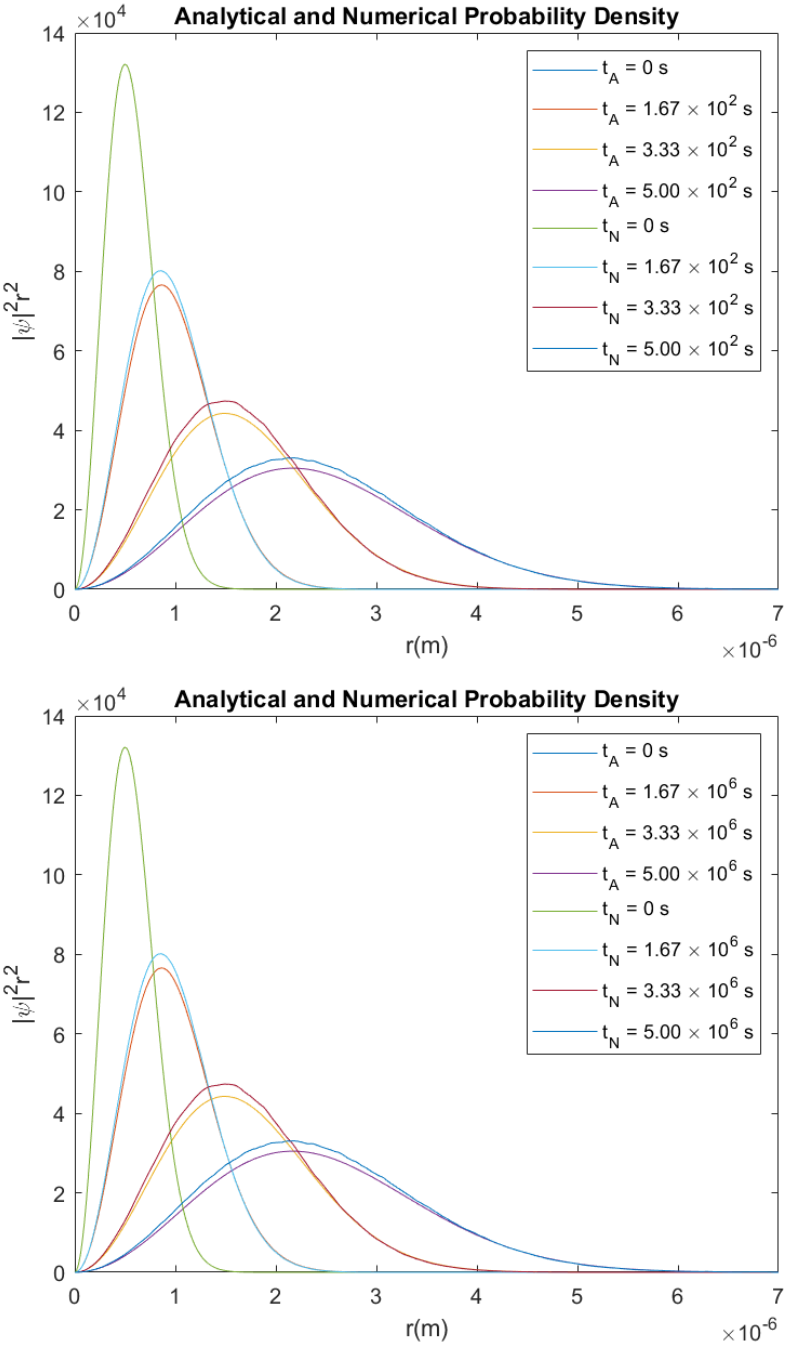

Figure 3.1: Comparison of the analytical and numerical probability density of a free particle of mass 5×10^{-20} kg (top) and 5×10^{-16} kg (bottom). Numerical infinity is at $r = 7\mu$m causing numerical curves to be slightly above the analytical ones.

3.2 The Spherical Potential Step

In this section, a step potential (also known as the Heaviside step function) will be used in the numerics. We will check the behaviour of the numerical results and see if it coincides with our theoretical understanding of the potential step. It is important to note that our initial wave function does not carry any initial momentum ($\langle p \rangle = 0$). Thus, the kinetic energy of the wave packet is just $(\Delta p)^2/2m$ which is always greater than 0. First, we consider the following potential step:

$$V(r,t) = \begin{cases} -V_0 & \text{for} \quad 0 \leq r \leq a \\ +V_0 & \text{for} \quad r > a \end{cases} \tag{3.2.1}$$

where V_0 and a are positive constants. Figure 3.2 shows the time evolution of the radial probability density in a potential step given by (3.2.1) at a finite distance of $a = 5\mu$m from the origin.

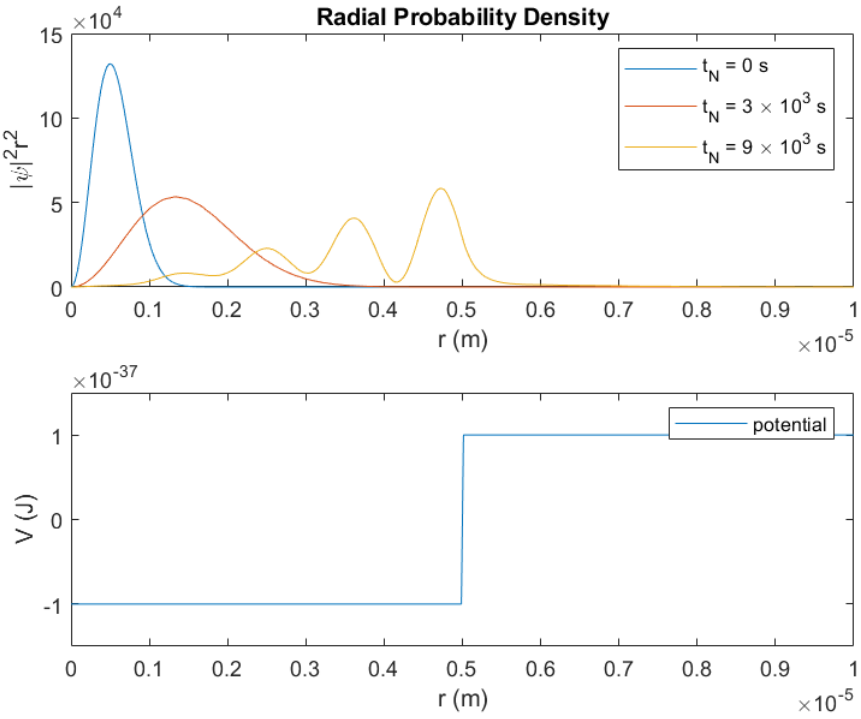

Figure 3.2: Radial probability density of a particle of mass 5×10^{-19} kg in a "step up" potential.

As one would expect, the wave packet is reflected by the potential barrier. Notice that the probability density does not vanish at the boundary $r = a$. Instead, it connects smoothly to the exponential decay in the region with the potential barrier.

The position of the potential step with respect to the origin a can be shifted up to the numerical infinity as shown in Figure 3.3. In the case of a approaching the numerical infinity (i.e., uniform potential), one would expect the wave packet to behave exactly the same way as in the case of a free particle.

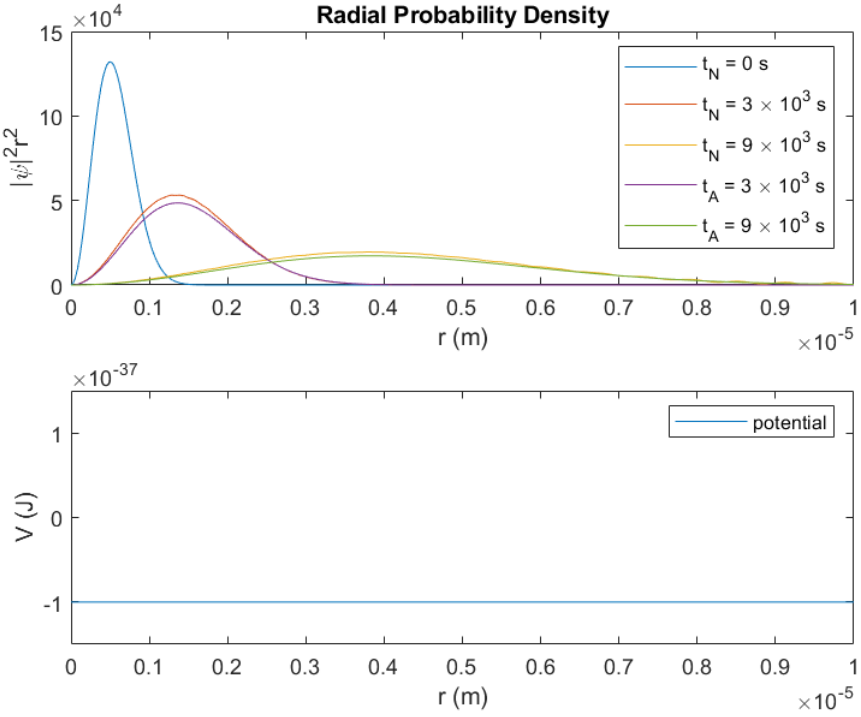

Figure 3.3: Radial probability density of a particle of mass 5×10^{-19} kg in a uniform potential.

We can also consider the case where the potential is a "step down" function given by:

$$V(r,t) = \begin{cases} -V_1 & \text{for} \quad 0 \leq r \leq a \\ -V_2 & \text{for} \quad r > a \end{cases} \tag{3.2.2}$$

where V_1 and V_2 are positive constants and $V_2 > V_1$. Classically, this can be thought of as an object moving from a region of high potential to a region of low potential. Thus,

one would expect the object to experience an acceleration and move faster in the region of lower potential. Figure 3.4 shows the evolution of the radial probability density in a potential step given by (3.2.2) at a finite distance of $a = 2\mu m$ from the origin.

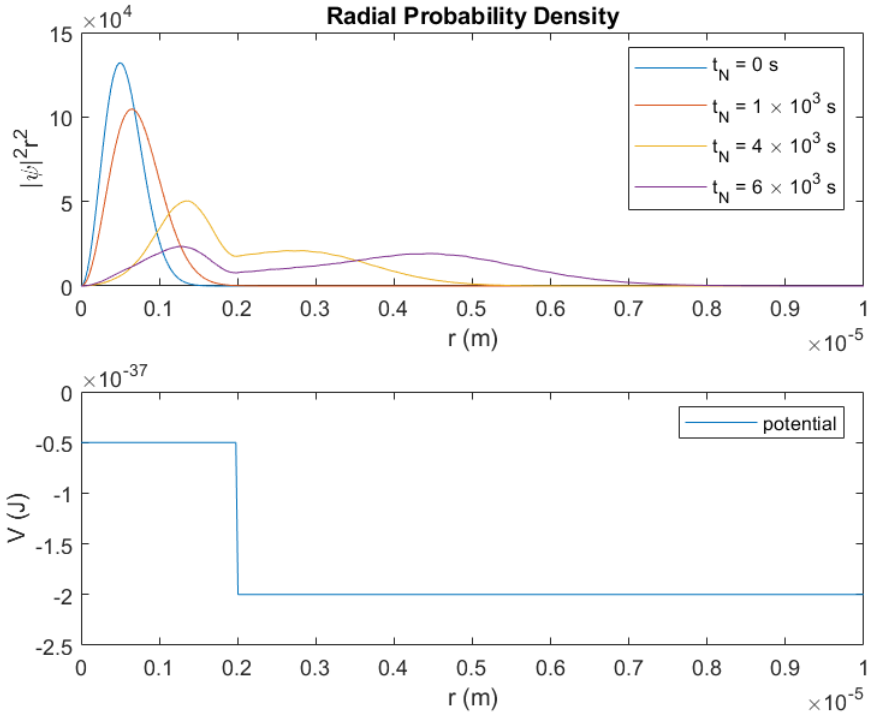

Figure 3.4: Radial probability density of a particle of mass 5×10^{-19} kg in a "step down" potential.

As can be seen from Figure 3.4, the probability is not fully transmitted into the region of low potential. Part of the probability is reflected by the potential well and moves towards the origin. This causes the wave function to form a superposition of two wave packets moving in opposite direction. This behaviour of the probability density is as predicted by the quantum scattering theory.

Chapter 4

Schrödinger-Newton Equation

In this chapter, we will use our programme to solve the Schrödinger-Newton equation. We will also explain the behaviour of the Gaussian wave packet evolving under the SN equation for different masses.

4.1 Summary of Results

We set the parameter α of our initial wave function to be 4×10^{12} m^{-2}, which corresponds to a Gaussian with an initial width of 0.5 μm. The following table shows the summary of the behaviour of the wave function for various masses with this particular value of α. Our numerical results are in good agreement with the results found by Giulini and Großardt [15].

Mass	Behaviour
Below 3×10^{-18} kg	Identical to free particle
3×10^{-18} kg to 1×10^{-17} kg	Spread slower than the free particle
$\sim 2 \times 10^{-17}$ kg	Oscillate
3×10^{-17} kg to 9×10^{-17} kg	Collapse towards the origin
1×10^{-16} kg to 4×10^{-16} kg	Chaotic
Above 5×10^{-16} kg	Stationary

Table 4.1: Summary of the results for SN equation with $\alpha = 4 \times 10^{12}$ m^{-2}.

4.2 The Behaviour of the Wave Function

The effects observed in the evolution of the probability density include the behaviour that one would expect physically, such as the spread and collapse of the wave function, and the effects that arise due to numerical artifacts, such as the chaotic and stationary behaviour of the wave function. They will now be analysed in detail.

4.2.1 Spread of the Wave Function

For a particle of mass in the order of 10^{-18} kg, its wave function evolving under the SN equation spreads slower compared to a free particle of the same mass. This is exactly what one would expect since the SN potential includes the attractive gravitational potential. Figure 4.1 shows the evolution of the probability density of a particle of mass 8×10^{-18} kg under the SN equation.

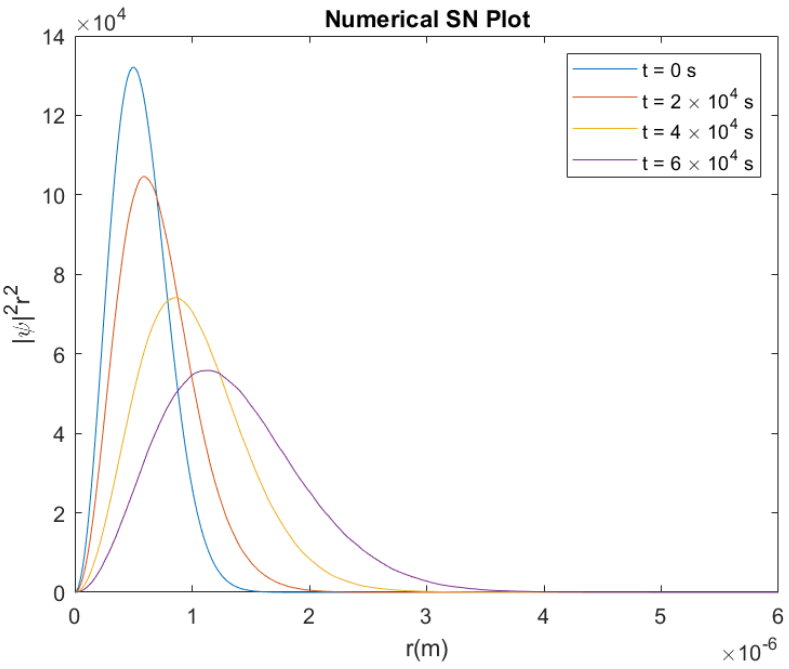

Figure 4.1: Radial probability density of a particle of mass 8×10^{-18} kg evolving under the SN equation.

We can also compare the position of the peak probability density of a particle of mass, say, 8×10^{-18} kg, evolving under the SN potential and the position of the peak probability density of the same particle evolving freely (i.e., zero potential) at different times.

Figure 4.2 shows that indeed the spread of the probability density is slower in SN model compared to the free particle.

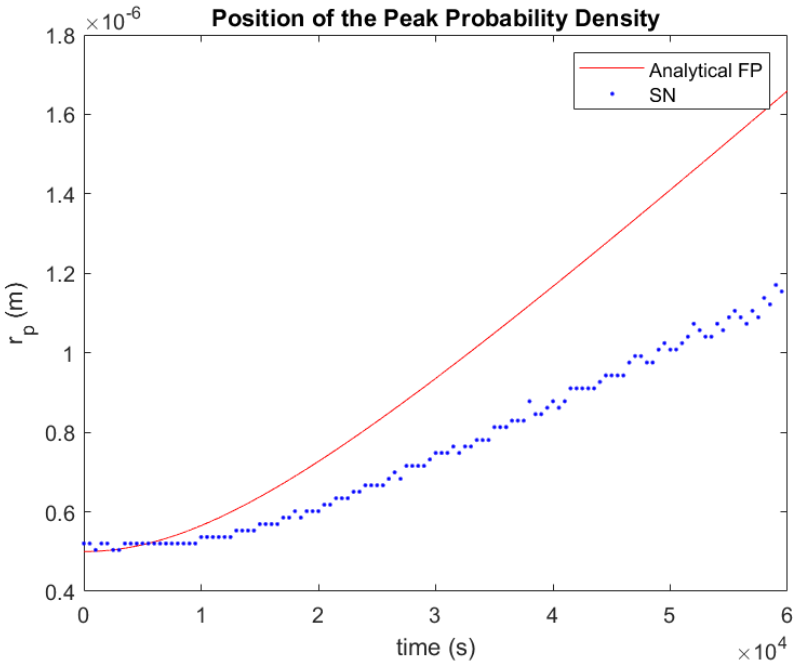

Figure 4.2: Comparison of the position of the peak probability density of a particle of mass 8×10^{-18} kg in the case of SN and free particle.

4.2.2 Oscillation of the Wave Function

The "oscillation" of the wave function can be roughly thought of as the situation where the position of the peak probability density moves around a specific distance. It is possible to make an estimation of the "critical mass", which is the mass where the contribution from the quantum wave packet dispersion is exactly the same as the contribution from the gravitational interaction. We follow the idea proposed by Carlip [16] in estimating the critical mass, that is, solving for the mass where the outward acceleration due to dispersion at the peak probability density is perfectly balanced by the inward acceleration due to gravitational interaction at time $t = 0$. The outward acceleration is given by (1.4.5) and the inward gravitational acceleration $a_g \sim Gm/r_p^2$. Thus, the accelerations will balance out at time $t = 0$ when the critical mass m_c is given by:

$$m_c \sim \left(\frac{\hbar^2\sqrt{\alpha}}{\mathcal{G}}\right)^{1/3} \tag{4.2.1}$$

For $\alpha = 4 \times 10^{12}$ m^{-2}, this gives $m_c \approx 7 \times 10^{-18}$ kg. As one can see, this estimation is not quite accurate. We can, however, improve it by applying Gauss's law for gravity and making use of the spherical symmetry in estimating the inward gravitational acceleration. Namely, the strength of the gravitational field at r_p is proportional to the mass within the radial distance $r < r_p$, which implies $a_g \sim G(\zeta m)/r_p^2$ where ζ is the fraction of mass within the radial distance $r < r_p$. Mathematically, ζ is given by:

$$\zeta = \int_0^{r_p} \rho(r,0) dr \int d\Omega \tag{4.2.2}$$

Substituting $\rho(r,0) = r^2|\psi(r,0)|^2$ and $r_p = \alpha^{-1/2}$ at time $t = 0$, we have

$$\zeta = \int_0^{\alpha^{-1/2}} r^2 \left(\frac{\alpha}{\pi}\right)^{\frac{3}{2}} e^{-\alpha r^2} dr \int d\Omega = \text{erf}(1) - \frac{2}{e\sqrt{\pi}} \approx 0.43 \tag{4.2.3}$$

With the correction term ζ, the critical mass m_c is given by:

$$m_c \sim \left(\frac{\hbar^2\sqrt{\alpha}}{\mathcal{G}\zeta}\right)^{1/3} \tag{4.2.4}$$

For $\alpha = 4 \times 10^{12}$ m^{-2}, we obtain $m_c \approx 9.2 \times 10^{-18}$ kg, which is a better estimation, i.e. closer to numerical findings. The discrepancy between our estimation and numerical results is not unlikely due to nonlinearities in the problem.

For our particular value of α, the oscillation of the wave function is observed for particles of mass approximately 2×10^{-17} kg. We know that the outward acceleration of the wave function $a_{out} \sim \hbar^2 r_p^{-3}/m^2$ and the inward acceleration $a_g \sim \mathcal{G} m r_p^{-2}$. Hence, for sufficiently small r_p, the outward acceleration dominates the inward acceleration and for sufficiently large r_p, the inward acceleration dominates the outward acceleration. This implies that there is a point in space where the two accelerations are equal, i.e., the equilibrium position r_{eq}. Suppose we have a wave function for which the peak probability density r_p moves initially towards the origin, i.e., r_p decreases over time. As r_p decreases over time, the outward acceleration grows faster than the inward acceleration. When the outward acceleration wins, the wave function starts to spread and r_p increases over time. As r_p increases over time, the outward acceleration decays faster than the inward acceleration and the wave function will start to move in again when the inward acceleration wins. This whole process repeats itself thus creating an "oscillating" wave function as shown in Figure 4.3.

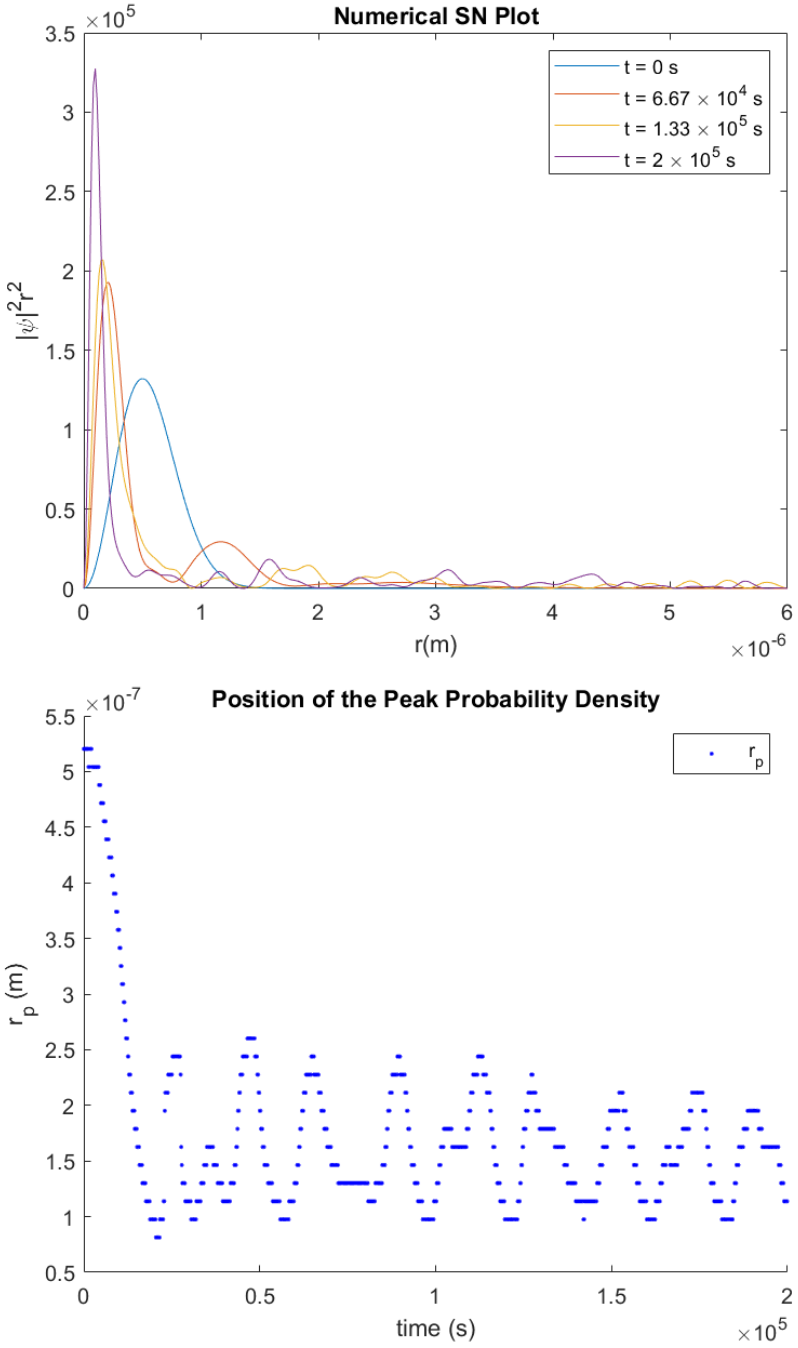

Figure 4.3: Radial probability density and position of the peak probability density of a particle of mass 2×10^{-17} kg evolving under the SN equation.

Having known the outward and inward acceleration up to a proportionality constant, we can solve for the "equilibrium" position r_{eq}, which is given by:

$$r_{eq} \sim \frac{\hbar^2}{\mathcal{G}m^3} \tag{4.2.5}$$

Equation (4.2.5) implies that if the mass of the particle m is large, r_{eq} is very close to the origin and thus, gravitational acceleration dominates nearly everywhere in space causing the wave function to gravitationally collapse. On the other hand, if the mass of the particle m is extremely small, r_{eq} is extremely far away from the origin and thus, the outward acceleration dominates nearly everywhere in space causing the wave function to spread.

4.2.3 Gravitational Collapse of the Wave Function

Figure 4.4 shows an example of the wave function "collapse" for a particle of mass 5×10^{-17} kg and $\alpha = 4 \times 10^{12}$ m^{-2}. By gravitational collapse we mean that the position of the peak probability density moves towards the origin.

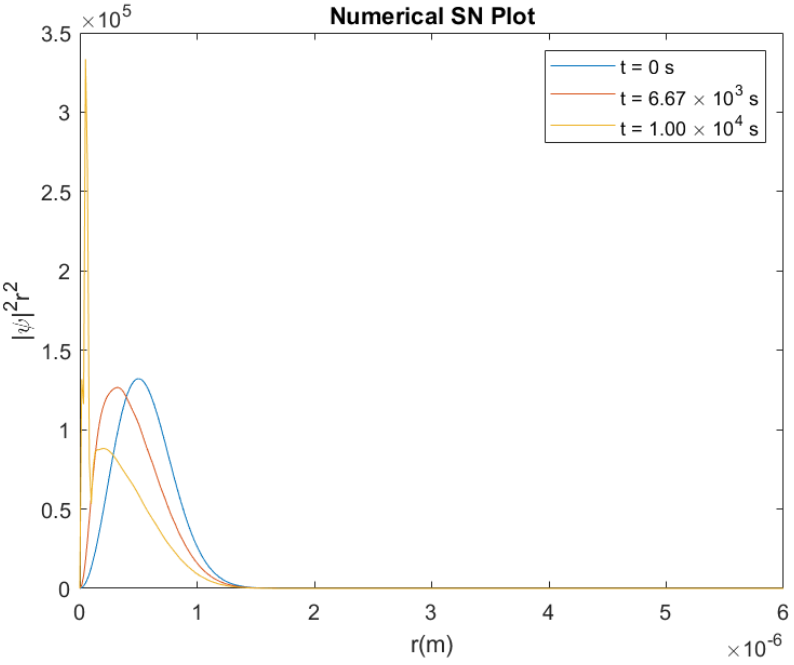

Figure 4.4: Radial probability density of a particle of mass 5×10^{-17} kg evolving under the SN equation.

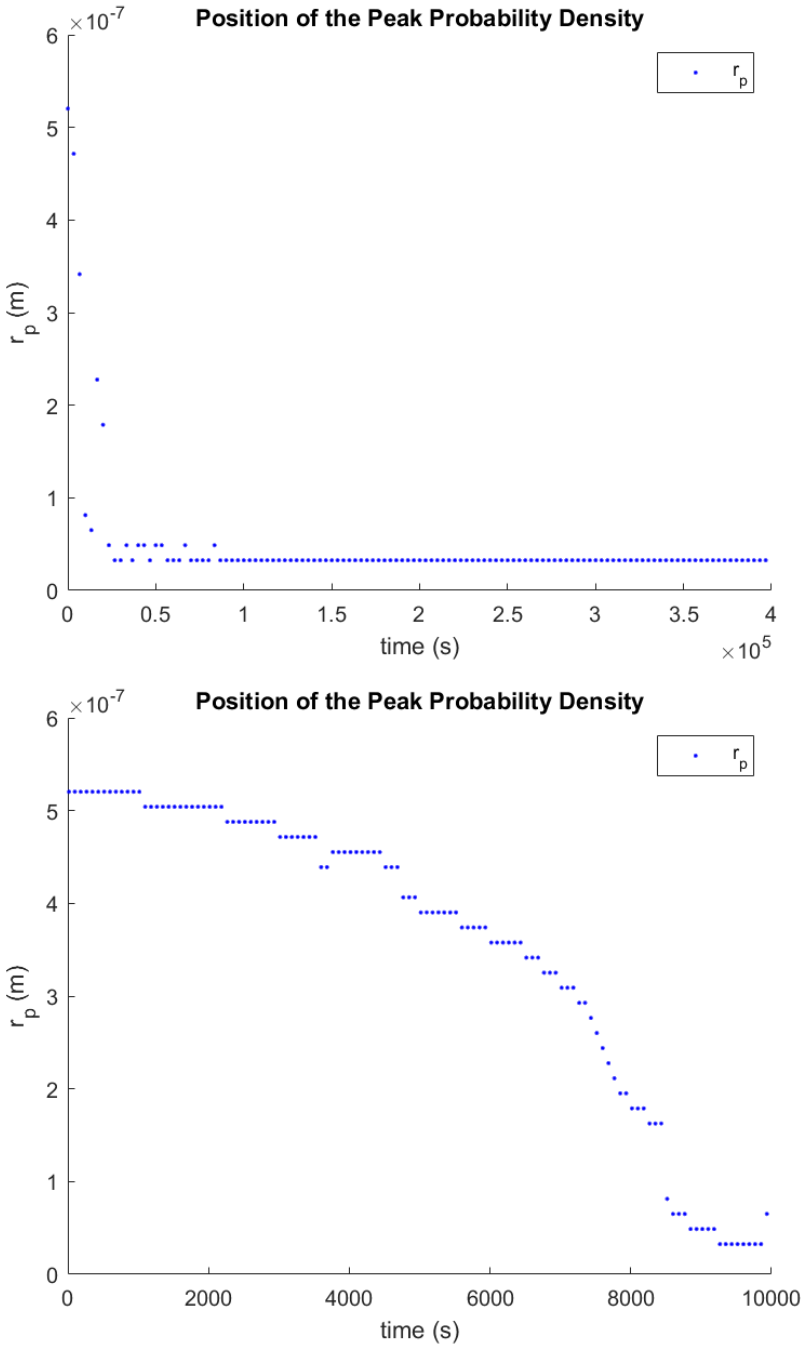

Figure 4.5: Position of the peak probability density of a particle of mass 5×10^{-17} kg evolving under the SN equation. Note different time scale on both plots. The top plot confirms that the peak probability density does not "oscillate".

In plotting the peak probability density as shown in Figure 4.5, one has to take note that the collapse of the wave function occurs quite rapidly compared to the other behaviour of the wave function. Figure 4.5 confirms rather nicely that the wave function collapses to some particular point near the origin.

4.2.4 Chaotic Behaviour

As the mass of the particle is increased beyond the collapse regime while fixing the parameter α, the wave function seemed to have a chaotic evolution as shown in Figure 4.6. In this regime, it is not possible to describe the behaviour of the wave function in simple terms. We currently do not know any physics relevant to this behaviour. Nonetheless, it is also possible that this behaviour of the wave function is a form of numerical artifact.

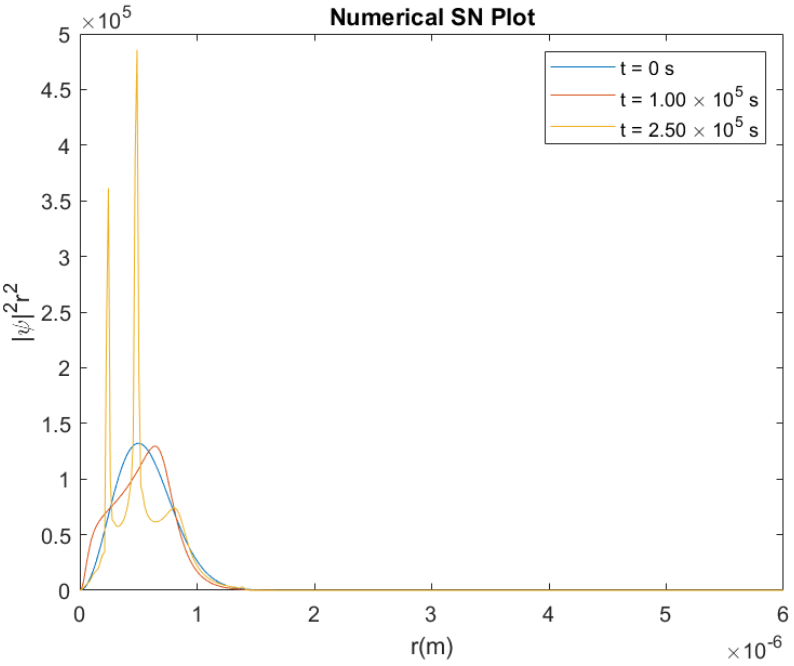

Figure 4.6: Radial probability density of a particle of mass 2×10^{-16} kg evolving under the SN equation.

4.2.5 Stationary Wave Function

The stationary behaviour of the wave function is observed for large masses (beyond the chaotic regime). The stationary behaviour means that the wave function does not evolve

over time at all, i.e., it remains identical to the initial wave function for any reasonable time range. As shown in Figure 4.7, the position of the peak probability density remains exactly at initial width of the wave function. Similar to the chaotic behaviour of the wave function, it is likely that this behaviour is a numerical artifact.

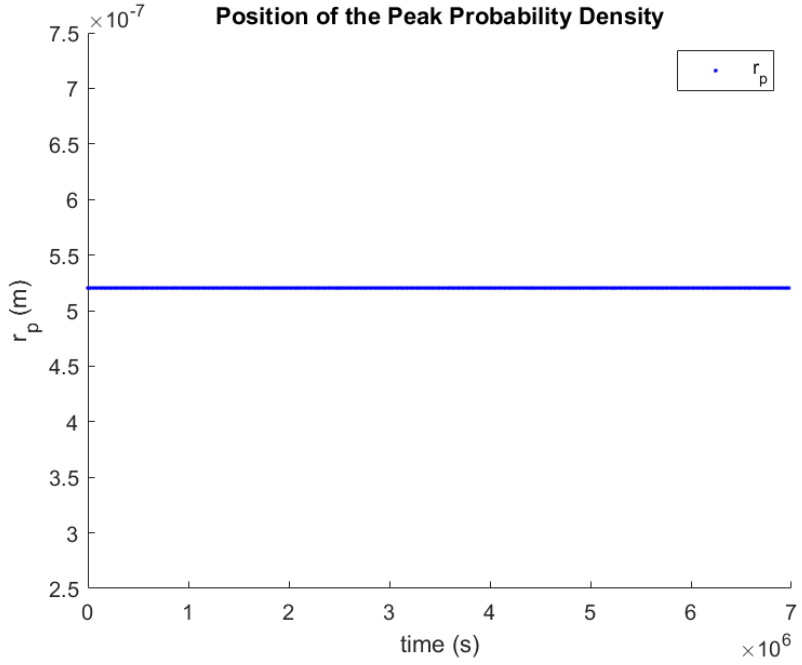

Figure 4.7: Position of the peak of probability density of a particle of mass 2×10^{-16} kg evolving under the SN equation.

4.3 The Schrödinger-Newton Potential

To give us a better understanding on the evolution of the wave function, it is useful to understand the overall shape of the SN potential and how it evolves over time. The relationship between the potential and the evolution of the wave function is highly non-linear, in the sense that the potential at time t depends on the wave function at time t but the wave function at time t itself depends on the potential at time t. However, in the case of the discretized SN equation, the wave function at a given timestep $n+1$ depends on the potential at timestep n, which in turn depends on the wave function at timestep n. Thus, using our knowledge of the behaviour of the wave packet in different types of potential steps (as discussed in Chapter 3), we can "visualize" the overall shape of the wave function at timestep $n+1$ given the potential and wave function at timestep n.

We will first consider the case of relatively small masses where the wave function spreads over time. Figure 4.8 shows the SN potential of a particle of mass 8×10^{-18} kg and $\alpha = 4 \times 10^{12}$ m^{-2} at different times.

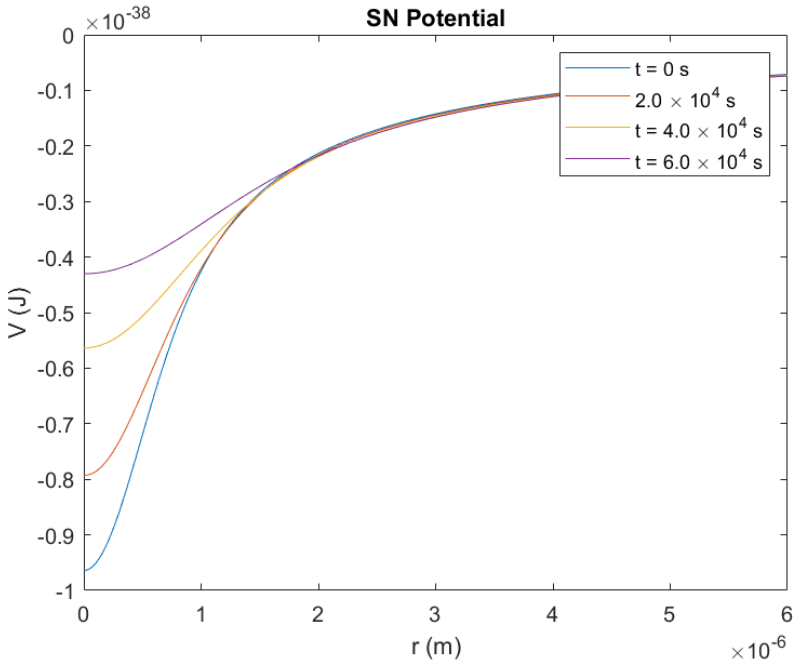

Figure 4.8: The SN potential of a particle of mass 8×10^{-18} kg at different times.

As shown in Figure 4.8, the SN potential has the form of a potential well. The depth of the potential well decreases over time causing the overall wave packet to spread. Due to the existence of this potential well in the SN model, the spread of the wave packet is slower compared to that of a free particle.

Figure 4.9 shows the SN potential of a particle of mass 2×10^{-17} kg which lies in the "oscillating" regime. The initial depth of the potential well grows deeper as the mass is increased which is as expected since the SN potential is directly proportional to the mass of the particle. Unlike the previous case where the depth of the potential well grows shallower over time, for a particle of mass $\sim 2 \times 10^{-17}$ kg, the depth of the potential well grows deeper over time and "oscillates" between a particular range of depths (as shown in Figure 4.9), in the sense that the depth of the well has the tendency to grow deeper or shallower at different points of time. This is not surprising recalling the fact that the

behaviour of the wave function evolution for this particular mass "oscillates" as well.

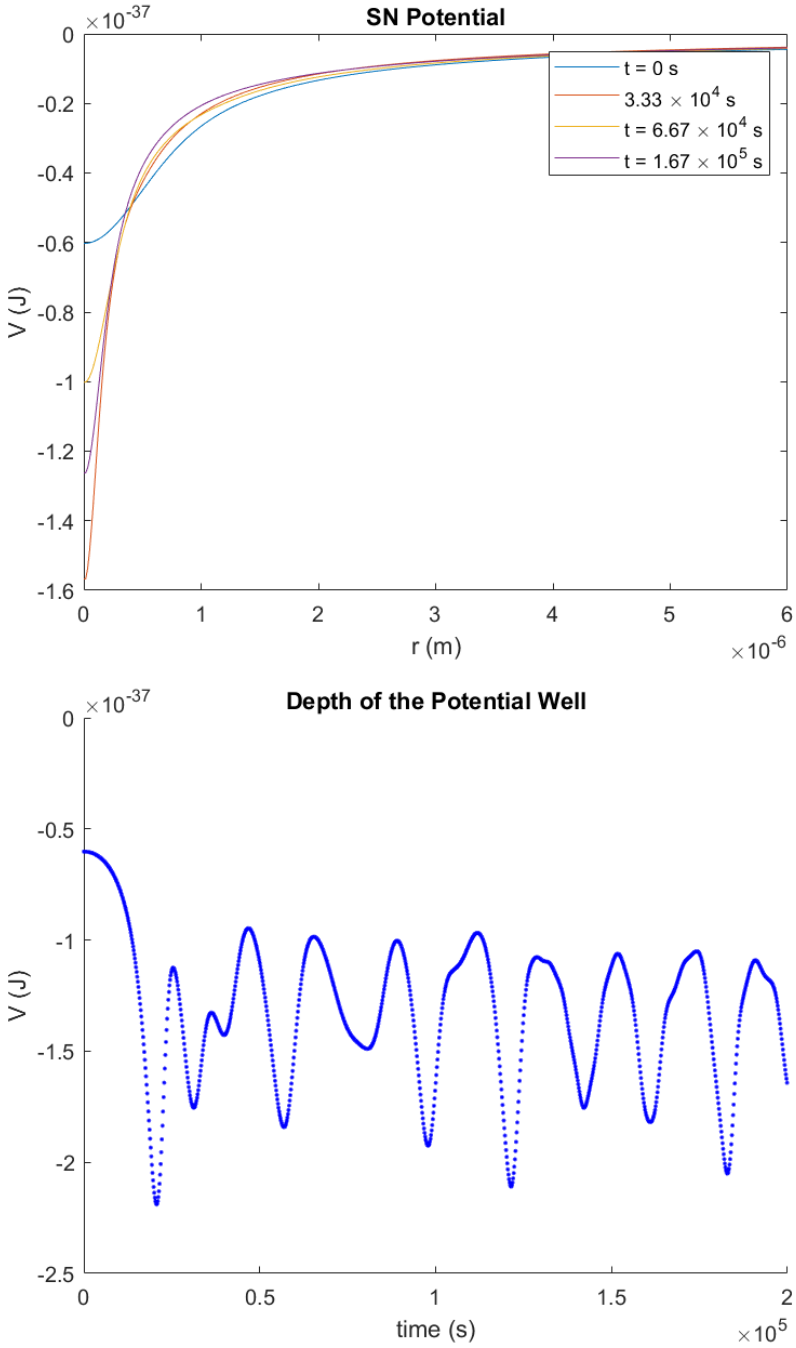

Figure 4.9: The SN potential and the depth of the potential well of a particle of mass 2×10^{-17} kg at different times.

Lastly, we consider the SN potential in the collapse regime as shown in Figure 4.10. The depth of the potential well grows deeper while the width of the well decreases over time. At sufficiently large time, the SN potential evolves into an extremely deep and narrow well. Thus, the wave packet evolving under this potential can be roughly thought of as being "trapped" in the deep and narrow well.

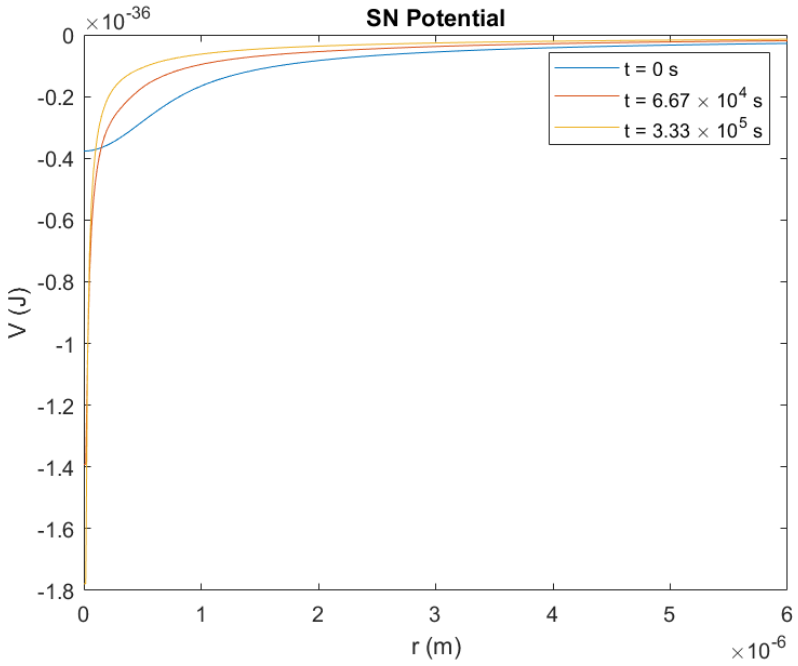

Figure 4.10: The SN potential of a particle of mass 5×10^{-17} kg at different times.

Chapter 5

Schrödinger-Newton-Lambda Equation

In this chapter, we will do a rough estimation of the parameters in our code so that the effects induced by the cosmological constant Λ are noticable and then use our programme to solve the Schrödinger-Newton-Lambda equation. Similar to the previous chapter, we will discuss the behaviour of the Gaussian wave packet evolving under the SNΛ equation.

5.1 Estimation of the Initial Gaussian Width

Since the cosmological constant Λ is extremely small (of the order of 10^{-52} m^{-2}), the effects induced by the cosmological constant are extremely hard to observe in our numerical results for any arbitrary choice of the initial Gaussian width. However, it is possible to make an estimate on the initial Gaussian width σ and the mass of the particle m such that the effects induced by the cosmological constant Λ are comparable to those of quantum mechanical dispersion and canonical gravitational interaction.

Given a spherically symmetric initial Gaussian wave function, the "total acceleration" a_{total} experienced by the peak of the probability density is approximately:

$$a_{\text{total}} \sim \frac{\hbar^2}{m^2\sigma^3} - \frac{\mathcal{G}m}{\sigma^2} + \frac{\Lambda c^2 \sigma}{3} \sim \frac{\lambda_C^2 c^2}{\sigma^3} - \frac{l_P^2 c^2}{\lambda_C \sigma^2} + \frac{\sigma c^2}{l_{dS}^2} \tag{5.1.1}$$

where λ_C is the Compton wavelength of the particle, $l_P = \sqrt{\hbar\mathcal{G}/c^2}$ is the Planck length, and $l_{dS} = \sqrt{3/\Lambda}$ is the de Sitter radius, which is of the order of 10^{26} m (comparable to the present day radius of the universe). We thus plot the curves of mass as a function of

width $m(\sigma)$ for two different cases: the quantum mechanical acceleration is of the same order as the dark energy acceleration and the gravitational acceleration is of the same order as the dark energy acceleration.

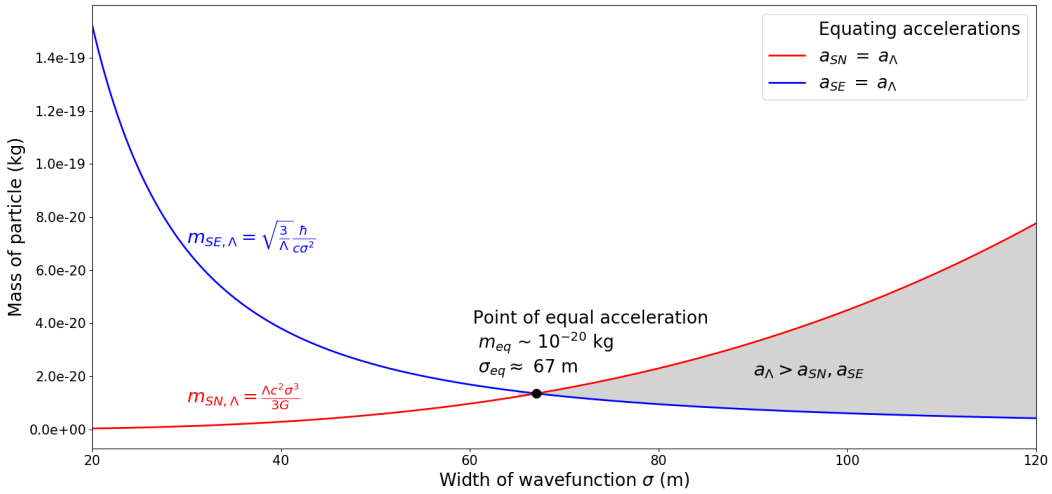

Figure 5.1: Relationship between the mass and width of the initial Gaussian so that the "acceleration" terms are of the same order. Acceleration due to quantum dispersion dominates acceleration due to dark energy below the $a_{\mathrm{SE}} = a_\Lambda$ curve. The gravitational acceleration dominates acceleration due to dark energy above the $a_{\mathrm{SN}} = a_\Lambda$ curve.

Figure 5.1 shows that the effects induced by the cosmological constant are dominating for a certain range of mass if the initial width of the Gaussian function is greater than ~ 67 m. Thus, for a Gaussian wave function with an initial width $\sigma > \sigma_{eq}$, one would expect the wave function to evolve identically to that of a free particle for relatively small masses since the "acceleration" induced by the dispersion of the wave packet dominates at this region. As the mass is increased, the "acceleration" induced by dark energy begins to dominate and we would expect to see its effects in this regime. For relatively large mass, one would expect the evolution of the wave function to reduce to the case of Schrödinger-Newton.

5.2 Summary of Results

We set the parameter α of our initial Gaussian wave function to be 1.78×10^{-4} m^{-2}, which corresponds to a Gaussian with an initial width of 75 m. Table 5.1 shows the

summary of the behaviour of the wave function evolving under the SNΛ equation for this particular choice of σ.

Mass	Behaviour
Below 1×10^{-21} kg	Identical to free particle
2×10^{-21} kg to 3×10^{-20} kg	Spread faster than the free particle
4×10^{-20} kg to 5×10^{-20} kg	Part of the wave function spreads slower while the other part spreads faster
6×10^{-20} kg to 1×10^{-19} kg	Part of the wave function collapses and "oscillates" while the other part spreads
$\sim 2 \times 10^{-19}$ kg	Chaotic
Above 3×10^{-19} kg	Stationary

Table 5.1: Summary of the results for SNΛ equation with $\alpha = 1.78 \times 10^{-4}$ m^{-2}.

For the purpose of comparison, Table 5.2 shows the summary of the behaviour of the wave function evolving under SN equation for $\alpha = 1.78 \times 10^{-4}$ m^{-2}.

Mass	Behaviour
Below 4×10^{-21} kg	Identical to free particle
5×10^{-21} kg to 2×10^{-20} kg	Spread slower than the free particle
3×10^{-20} kg to 5×10^{-20} kg	"Oscillates"
6×10^{-20} kg to 1×10^{-19} kg	Collapse
2×10^{-19} kg to 2×10^{-18}	Chaotic
Above 2×10^{-18} kg	Stationary

Table 5.2: Summary of the results for SN equation with $\alpha = 1.78 \times 10^{-4}$ m^{-2}.

From Table 5.1 and 5.2, one can tell that the numerical results might no longer be valid due to numerical artifacts when the mass of the particle is greater than 2×10^{-19} kg. Some interesting dynamics, such as the "partial spread" and "partial collapse" of the wave function, are observed in the case of the SNΛ potential. Especially that they are not present in the case of the SN potential.

5.3 The Behaviour of the Wave Function

We will only discuss the "unique" effects observed in the evolution of the wave function under the SNΛ equation (i.e. behaviour which is not present in the case of Schrödinger-Newton).

5.3.1 Spread of the Wave Function

For our particular choice of α, the wave function of a particle with a mass in the range of 2×10^{-21} kg to 3×10^{-20} kg evolving under the SNΛ equation spreads faster compared to a free particle of the same mass. This behaviour is as what one would expect to keep in mind the fact that the dark energy term in the potential acts as an anti-gravity, i.e. repulsively. In this range of mass, the effects induced by dark energy are stronger than the effects induced by gravitational interaction.

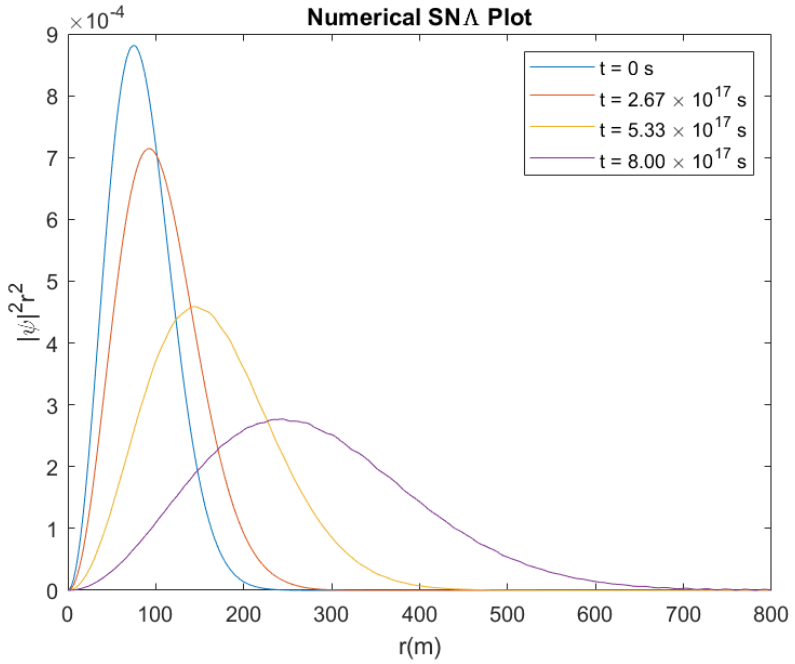

Figure 5.2: Radial probability density of a particle of mass 1×10^{-20} kg evolving under the SNΛ potential. Note macroscopic spatial dimensions and extremely long evolution times.

Figure 5.3 shows that the spread of the wave function for this particular mass is indeed faster than the case of a free particle of the same mass.

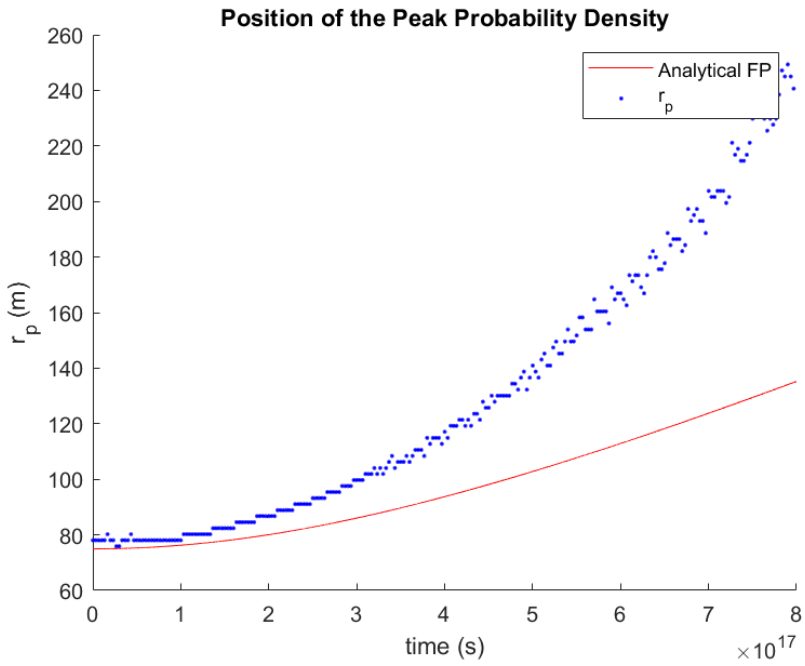

Figure 5.3: The position of the peak probability density of a particle of mass 1×10^{-20} kg evolving under the SNΛ potential increases faster than in the case of a free particle of the same mass.

5.3.2 "Partial Spread" of the Wave Function

As the mass of the particle is increased, the effects induced by gravitational interaction start to play a significant role in the evolution of the wave function. The gravitational potential is proportional to the inverse of the radial distance whereas the potential induced by dark energy is proportional to the square of the radial distance. Thus, the effects induced by gravitational interaction are dominant for relatively small radial distance and the effects induced by dark energy are dominant for relatively large radial distance. If this is indeed the case, given a Gaussian wave packet with sufficiently large initial width, one could expect part of the wave packet with relatively small radial distance to collapse and part of the wave packet with relatively large radial distance to spread. More generally, it is possible for the initial wave packet to decay into two wave packets with different behaviour. Part of the wave packet with relatively small radial distance tends to exhibit the effects observed in the SN model, such as the "oscillations" or slower spread, whereas the other part of wave function with relatively large radial distance, tends to spread faster than in the case of the free particle.

Figure 5.4 shows an example of the wave packet of a particle of mass 5×10^{20} kg decaying into two wave packets that spread with different rates. Part of the wave packet with a smaller radial distance spreads slower compared to the part of the wave packet with larger radial distance.

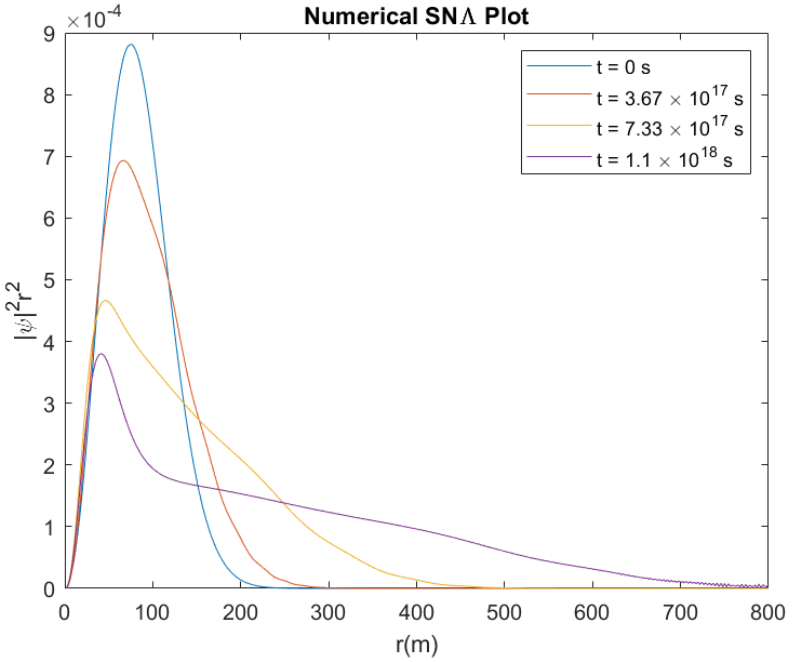

Figure 5.4: Radial probability density of a particle of mass 5×10^{-20} kg evolving under the SNΛ potential.

5.3.3 "Partial Collapse" of the Wave Function

The "partial collapse" of the wave function describes the behaviour of the wave packet where part of the wave packet with relatively small radial distance collapses and "oscillates" as explained previously in the SN model whereas the other part of the wave packet with relatively large radial distance spreads away. For particles of mass between 6×10^{-20} kg and 8×10^{-20} kg, the effects induced by gravitational interaction are sufficiently large such that part of the wave packet with relatively small radial distance does not spread over time. Figure 5.5 shows an example of this behaviour exhibited by a particle of mass 6×10^{-20} kg.

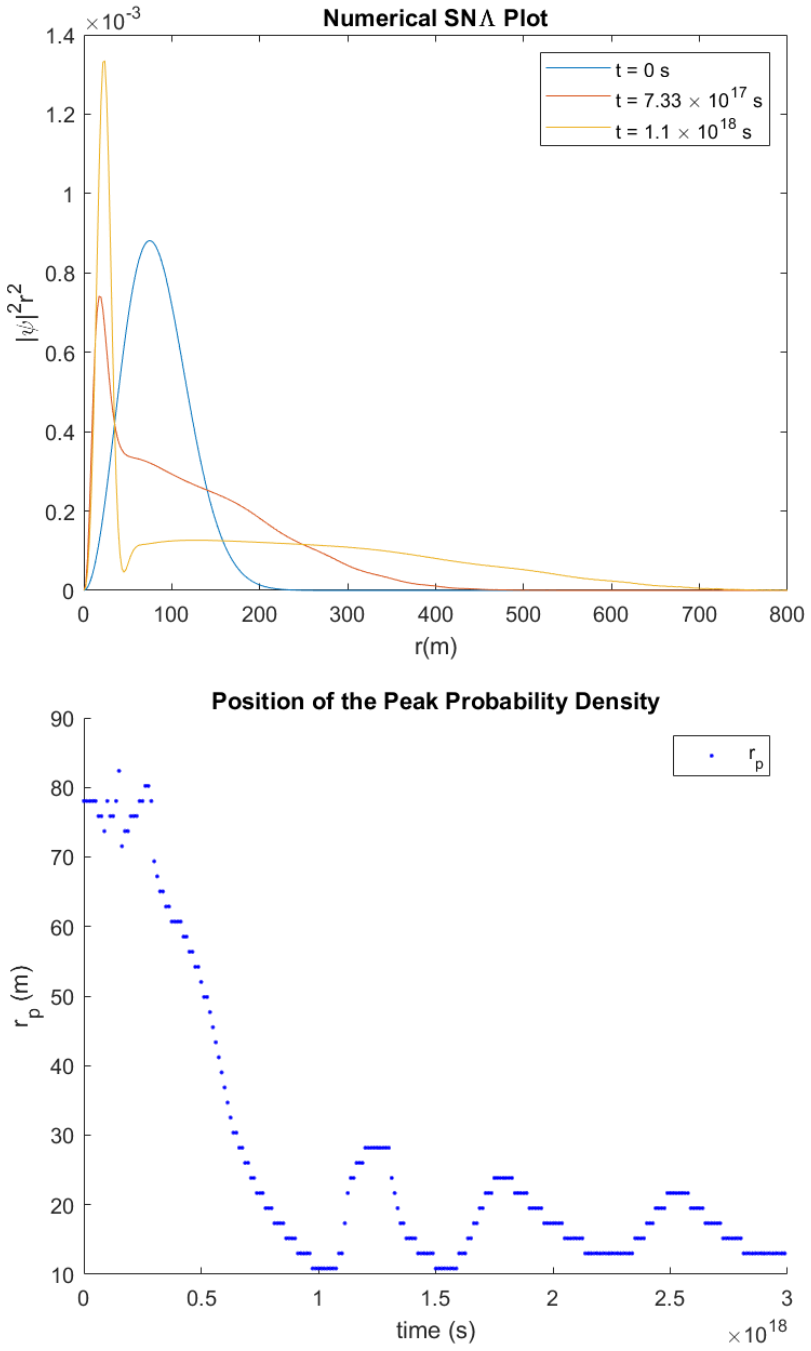

Figure 5.5: Radial probability density and position of the peak probability density of a particle of mass 6×10^{-20} kg evolving under the SNΛ potential.

For comparison, Figure 5.6 shows the behaviour of the same particle evolving under SN

potential. In the case of SN potential, the initial wave packet does not decay into two wave packets.

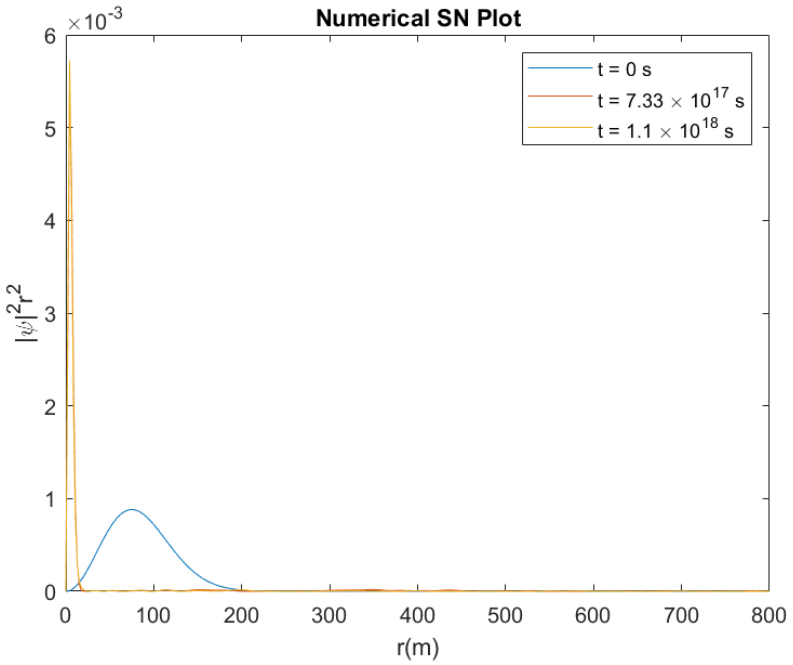

Figure 5.6: Radial probability density of a particle of mass 6×10^{-20} kg evolving under the SN potential.

As the mass of the particle is further increased, the fraction of the wave function that previously spreads decreases gradually and the collapse of the wave function occurs more rapidly. The frequency of the "oscillations" of the wave function increases while the amplitude of the "oscillations" decreases as the mass of the particle is increased. This can be seen by comparing Figure 5.7 to Figure 5.5.

We would expect for sufficiently large mass, the fraction of the wave function that spreads away would vanish so that the gravitational collapse of the entire wave function could be observed as in the case of the SN model. In other words, for our particular choice of α, the evolution of the wave function under the SNΛ equation must reduce to the evolution under the SN equation for sufficiently large mass. However, we were not able to reach this regime with the present numerical procedures.

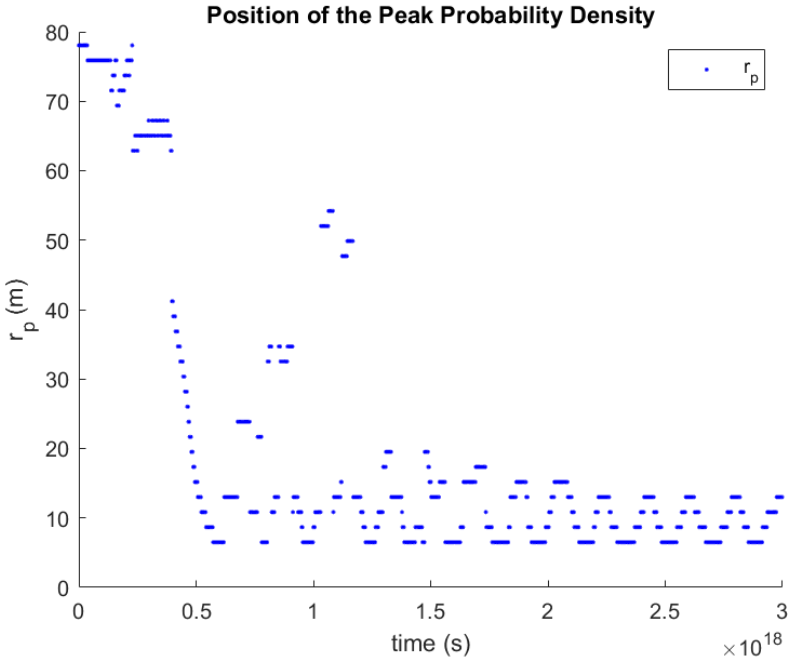

Figure 5.7: Position of the peak probability density of a particle of mass 9×10^{-20} kg evolving under the SNΛ potential.

5.4 The Schrödinger-Newton-Lambda Potential

Similar to the previous chapter, we will try to better understand the behaviour of the wave function evolution under the SNΛ model by looking at the SNΛ potential.

We first consider the case in which the wave packet spreads, i.e., the wave function of particles of mass between 5×10^{-21} kg and 2×10^{-20} kg. As shown in Figure 5.8, the potential corresponding to this particular range of mass does not change significantly over time since the potential is dominated by the contribution from dark energy (recall that only the "SN term" in the potential is time dependent). Based on the shape of the potential, one can deduce that the SNΛ potential corresponding to this particular range of mass is a repulsive potential, explaining the faster spread of the wave packet compared to the case of the free particle. Figure 5.9 shows that the effects induced by dark energy are more prominent for relatively larger mass. This implies that the spread of a wave packet corresponding to a relatively large mass is faster than the spread of the same wave packet corresponding to a relatively small mass. The effect opposite to the canonical quantum theory.

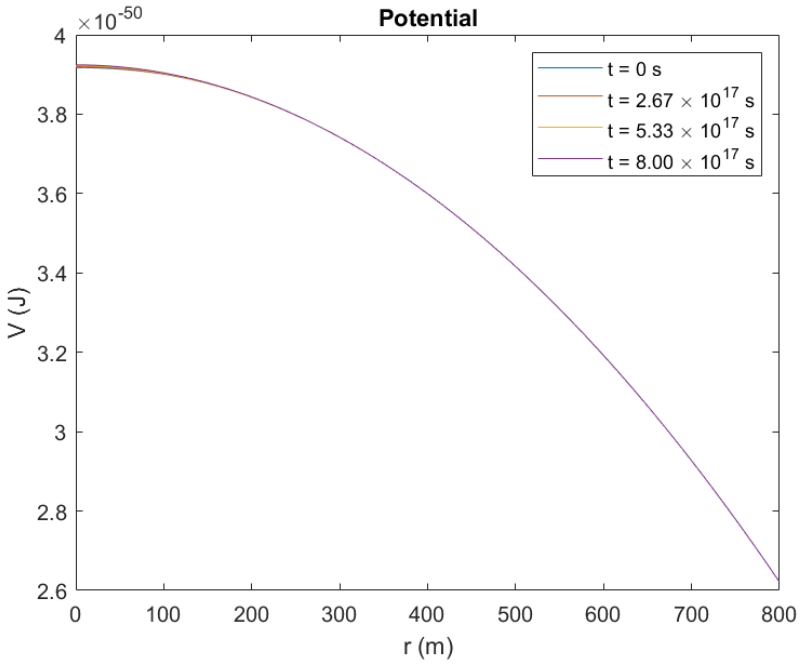

Figure 5.8: The SNΛ potential of a particle of mass 1×10^{-20} kg at different times.

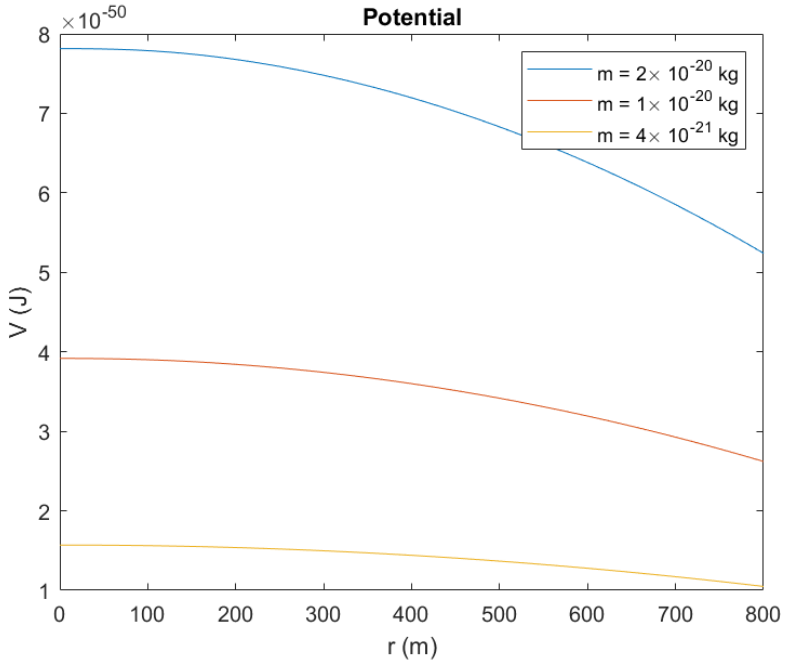

Figure 5.9: The SNΛ potential of particles of different masses at time $t = 0$.

Figure 5.10 shows the evolution of the SNΛ potential of a particle of mass 5×10^{-20} kg. The potential corresponding to this particular mass evolves to form a shallow well at the region with relatively small radial distance. This potential well is not sufficiently deep to collapse part of the wave function. However, the part of the wave function which is affected by this potential well experience a slower spread compared to the rest of the wave function (as shown in Figure 5.4).

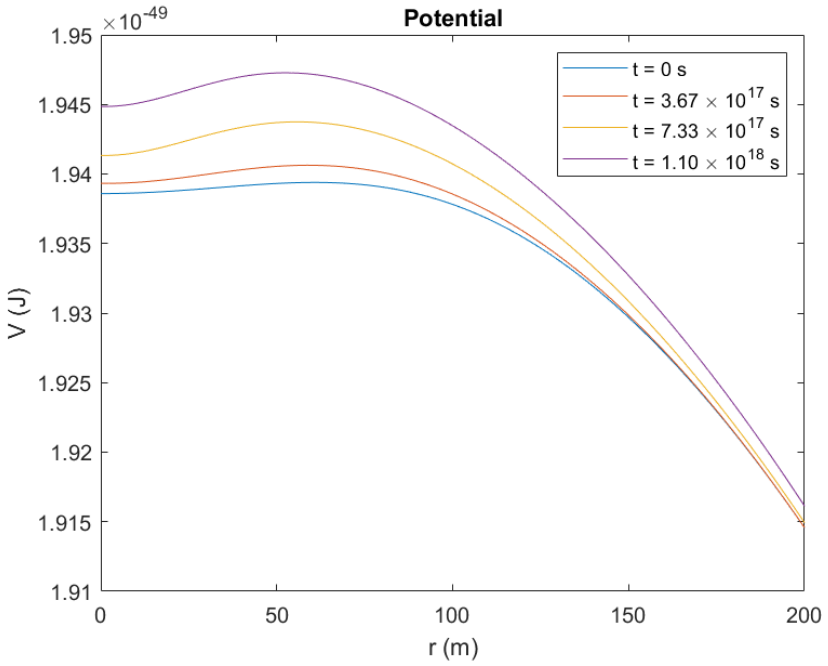

Figure 5.10: The SNΛ potential of a particle of mass 5×10^{-20} kg at different times.

Let us now increase further the mass of the particle to 6×10^{-20} kg (the evolution of the probability density corresponding to this particular mass is shown in Figure 5.5). The potential corresponding to this particular mass evolves to form a potential well as shown in Figure 5.11. In this case, the potential well is sufficiently deep to collapse part of the wave function. In order to have an entire wave function collapse, the initial width of the potential well must be greater than the width of the wave function. This condition can only be achieved if the mass is increased further. However, as we have mentioned earlier, numerical artifacts start to be significant before a sufficiently large mass can be used to observe the entire collapse of the wave function.

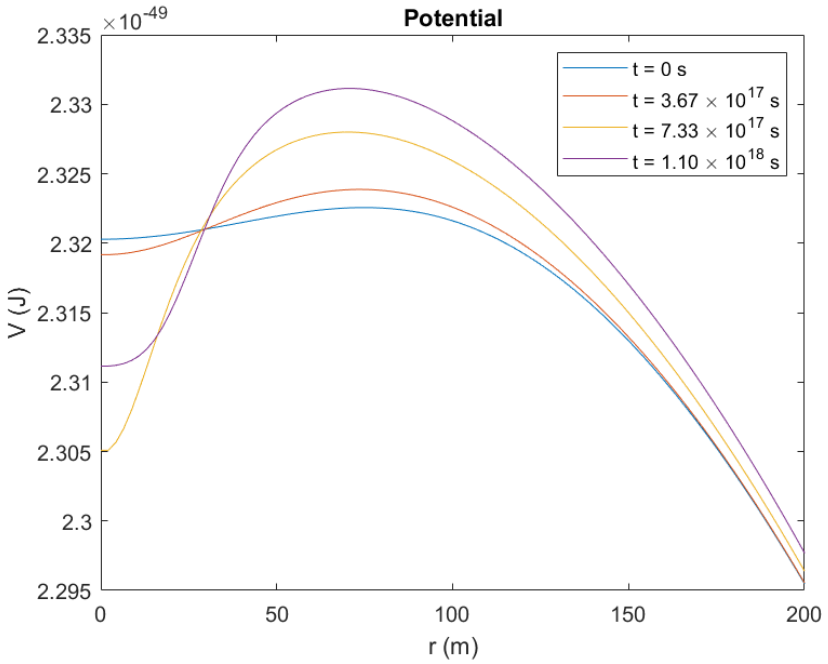

Figure 5.11: The SNΛ potential of a particle of mass 6×10^{-20} kg at different times.

5.5 The Concept of the Turn-Around Radius

In a dark energy universe as described by the ΛCDM model, there is a maximum radius of a spherical mass distribution above which the mass no longer collapses but disperses due to the expansion of the universe. The radius which marks the boundary between the attractive and repulsive behaviour is known as the turn-around radius [17]. Thus, if the SNΛ model predicts a turn-around radius smaller than the initial Gaussian width for a certain mass, we would expect the wave packet to be unstable in the framework of the SNΛ model (i.e., the entire wave packet will not collapse). Classically, the turn-around radius in the case of a Schwarzschild-de Sitter spacetime [1] is given by

$$R_{TA} = \left(\frac{3\mathcal{G}M}{\Lambda c^2}\right)^{1/3} \tag{5.5.1}$$

For a mass of 6×10^{-20} kg, the turn-around radius is approximately 10^2 m. Eq. (5.5.1) does not take into account the contribution from quantum mechanical dispersion. Thus,

[1] The Schwarzschild-de Sitter spacetime is a spherically symmetric solution to Einstein's field equations with a positive cosmological constant.

we would expect the turn-around radius predicted by the SNΛ model to be smaller than the classical turn-around radius. It would be interesting if one could measure the actual turn-around radius from experiments and compare it to our numerical results.

5.6 Conclusions and Future Work

In this thesis, we have investigated the solutions to the existing Schrödinger-Newton equation numerically. We have also extended the numerical method based on the works in [12] to investigate the solutions to the Schrödinger-Newton-Lambda equation, a modified Schrödinger-Newton equation which includes the effects induced by dark energy in the form of a positive cosmological constant.

We recovered the behaviour of a wave packet evolving under the Schrödinger-Newton model, such as the (slower) spread and the gravitational collapse of the wave packet. For the case of the Schrödinger-Newton-Lambda model, we were able to observe interesting new behaviour, such as the (faster) spread, the "partial spread" and the "partial collapse" of the wave packet. These results are not surprising recalling the nature of dark energy, which behaves as an anti-gravity. In addition, the relevant mass and length scales which one can use to test the effects induced by dark energy were obtained as well. It turned out that one has to superpose a particle of mass of the order of 10^{-20} kg over the distance above 50 m, which is extremely challenging in practice. Furthermore, the evolution of the wave function under the Schrödinger-Newton-Lambda model is extremely long (of the order of 10^{17} s). Therefore, it is extremely challenging for one to come up with an experiment to test the effects induced by the cosmological constant in this collapse model approach.

There is still plenty of work to be done regarding the Schrödinger-Newton-Lambda equation. For instance, it would be interesting to consider the case of two or more particles in the Schrödinger-Newton-Lambda model and investigate the interaction between them and compare the behaviour to that of macroscopic objects in a dark energy universe.

Appendix A

Newtonian Limit of Einstein's Field Equations

Here, we derive in detail the Poisson's equation (1.2.5) from the semiclassical approach by Møller and Rosenfeld and solve the Poisson's equation using the method of Green's function. Similar derivations, namely the Newtonian limit of Einstein's equations without the cosmological constant, can be found in textbooks on General Relativity [11].

A.1 Derivation of Poisson's Equation for the Potential in the Newtonian Limit

We begin by writing our starting point (1.2.1):

$$R_{\mu\nu} - \frac{1}{2}Rg_{\mu\nu} + \Lambda g_{\mu\nu} = \frac{8\pi\mathcal{G}}{c^4} \langle\psi| \hat{T}_{\mu\nu} |\psi\rangle \tag{A.1.1}$$

where $R_{\mu\nu}$ is the Ricci tensor, $g_{\mu\nu}$ is the metric tensor, and R is the Ricci scalar. The approach to reduce Einstein's field equations is to invoke the following assumptions:

1. We assume that the gravitational field is static. This implies that any time derivative component will vanish.

2. We invoke that spacetime is nearly flat with some small perturbations. Mathematically, we can write

$$g_{\mu\nu} = \eta_{\mu\nu} + h_{\mu\nu} \tag{A.1.2}$$

where $\eta_{\mu\nu}$ is the Minkowski metric, with signature $(-,+,+,+)$ and $|h_{\mu\nu}| \ll 1$ can be treated as small perturbations. We will ignore second order and higher terms in $h_{\mu\nu}$.

3. We assume that the field due to pressure is negligible compared to the field due to mass density. This implies that the component $\hat{T}_{00} = \hat{\rho}c^2$ is dominant and we will only consider this component.

Taking the trace of Einstein's field equations on both sides gives us:

$$R - \frac{1}{2}Rg^{\mu\nu}g_{\mu\nu} + \Lambda g^{\mu\nu}g_{\mu\nu} = \frac{8\pi\mathcal{G}}{c^4}\langle\psi|\,\hat{T}\,|\psi\rangle \tag{A.1.3}$$

Since $g^{\mu\nu}g_{\mu\nu} = \delta^{\mu}_{\mu} = 4$, we have

$$R = -\frac{8\pi\mathcal{G}}{c^4}\langle\psi|\,\hat{T}\,|\psi\rangle + 4\Lambda \tag{A.1.4}$$

Substituting (A.1.4) into (A.1.1) and rewriting gives:

$$R_{\mu\nu} = \frac{8\pi\mathcal{G}}{c^4}\left(\langle\psi|\,\hat{T}_{\mu\nu}\,|\psi\rangle - \frac{1}{2}\langle\psi|\,g_{\mu\nu}\hat{T}\,|\psi\rangle\right) + \Lambda g_{\mu\nu} \tag{A.1.5}$$

The Ricci tensor can be obtained by contracting the Riemann tensor. In terms of Christoffel symbols, the Ricci tensor reads

$$R_{\mu\nu} = g^{\alpha\beta}R_{\beta\mu\alpha\nu} = \partial_\alpha\Gamma^{\alpha}_{\nu\mu} - \partial_\nu\Gamma^{\alpha}_{\mu\alpha} + \Gamma^{\alpha}_{\alpha\beta}\Gamma^{\beta}_{\nu\mu} - \Gamma^{\alpha}_{\nu\beta}\Gamma^{\beta}_{\alpha\mu} \tag{A.1.6}$$

The dominant term of the Ricci tensor in the static weak-field limit can be expressed as

$$R_{00} = \partial_\alpha\Gamma^{\alpha}_{00} - \partial_0\Gamma^{\alpha}_{0\alpha} + \Gamma^{\alpha}_{\alpha\beta}\Gamma^{\beta}_{00} - \Gamma^{\alpha}_{0\beta}\Gamma^{\beta}_{\alpha0} \tag{A.1.7}$$

The second term of (A.1.7) is a time derivative which vanishes for a static field. The third and fourth terms are second order in $g_{\mu\nu}$ and hence are negligible. Thus, to the first order in $g_{\mu\nu}$,

$$R_{00} = \partial_\alpha\Gamma^{\alpha}_{00} \tag{A.1.8}$$

The Christoffel symbols read

$$\Gamma^{\mu}_{\alpha\beta} = \frac{1}{2}g^{\mu\nu}\left(\partial_\beta g_{\nu\alpha} + \partial_\alpha g_{\nu\beta} - \partial_\nu g_{\alpha\beta}\right) \tag{A.1.9}$$

Thus, Γ^{μ}_{00} can be calculated as follows (keeping only linear terms of the perturbation and ignoring time derivatives):

$$\Gamma^{\mu}_{00} = \frac{1}{2}g^{\mu\nu}\left(\partial_0 g_{\nu 0} + \partial_0 g_{\nu 0} - \partial_\nu g_{00}\right) = \frac{1}{2}\left(\eta^{\mu\nu} - h^{\mu\nu}\right)\left(-\partial_\nu h_{00}\right) = -\frac{1}{2}\eta^{\mu\nu}\partial_\nu h_{00} \quad \text{(A.1.10)}$$

Hence, (A.1.8) becomes

$$R_{00} = -\frac{1}{2}\eta^{\mu\nu}\partial_\mu\partial_\nu h_{00} \quad \text{(A.1.11)}$$

Under the assumptions of the static weak-field limit, (A.1.5) can be written as

$$R_{00} = \frac{8\pi\mathcal{G}}{c^4}\left(\langle\psi|\,\hat{T}_{00}\,|\psi\rangle - \frac{1}{2}\langle\psi|\,g_{00}\hat{T}\,|\psi\rangle\right) + \Lambda g_{00} \quad \text{(A.1.12)}$$

The trace of $\hat{T}_{\mu\nu}$, to the lowest nontrivial order, can be found by the contraction:

$$\hat{T} = g^{\mu\nu}\hat{T}_{\mu\nu} = g^{00}\hat{T}_{00} = -\hat{\rho}c^2 \quad \text{(A.1.13)}$$

Substituting (A.1.13) into (A.1.12) yields:

$$R_{00} = \frac{4\pi\mathcal{G}}{c^2}\langle\psi|\,\hat{\rho}\,|\psi\rangle - \Lambda \quad \text{(A.1.14)}$$

Combining (A.1.11) and (A.1.14), we find:

$$\eta^{\mu\nu}\partial_\mu\partial_\nu h_{00} = -\frac{8\pi\mathcal{G}}{c^2}\langle\psi|\,\hat{\rho}\,|\psi\rangle + 2\Lambda \quad \text{(A.1.15)}$$

The only nonzero terms of the Minkowski metric are on the diagonals and since the term with time derivative $\partial_0 h_{00}$ is also zero, the nonzero terms are, therefore, those with double spatial indices.

$$\partial_1\partial_1 h_{00} + \partial_2\partial_2 h_{00} + \partial_3\partial_3 h_{00} = \nabla^2 h_{00} = -\frac{8\pi\mathcal{G}}{c^2}\langle\psi|\,\hat{\rho}\,|\psi\rangle + 2\Lambda \quad \text{(A.1.16)}$$

Substituting $h_{00} = -2\Phi/c^2$ into (A.1.16) gives:

$$\nabla^2\Phi = 4\pi\mathcal{G}\langle\psi|\,\hat{\rho}\,|\psi\rangle - \Lambda c^2 = 4\pi\mathcal{G}m|\psi|^2 - \Lambda c^2 \quad \text{(A.1.17)}$$

Here, $\hat{\rho} = m\,|\vec{r}\rangle\langle\vec{r}|$ is the mass density operator.

A.2 Solution to Poisson's Equation: Method of Green's Function

We will briefly discuss the method of Green's function to solve Poisson's equations. Consider the following Poisson's equation:

$$\nabla^2 u(\vec{r}) = \rho(\vec{r}) \tag{A.2.1}$$

Suppose we have the solution to the equation:

$$\nabla^2 G(\vec{r}, \vec{r}') = \delta^3(\vec{r} - \vec{r}') \tag{A.2.2}$$

where the function $G(\vec{r}, \vec{r}')$ is known as the Green's function. It can be thought of as the response of the system to a soure at $\vec{r} = \vec{r}'$. Given some function $\rho(\vec{r})$, which can be expressed in terms of a summation of delta functions, we can find a solution by summing up all the response to such sources. Mathematically,

$$u(\vec{r}) = \int G(\vec{r}, \vec{r}')\rho(\vec{r}')d^3\vec{r}' \tag{A.2.3}$$

We can show that (A.2.3) is indeed a solution to (A.2.1) by substituting directly (A.2.3) into (A.2.1). Now, we integrate (A.2.2) over a sphere of radius R centered at $\vec{r}'$ with respect to $\vec{r}$.

$$\int_V \nabla^2 G\left(\vec{r}, \vec{r}'\right) dV = 1 \tag{A.2.4}$$

By the divergence theorem, the left hand side of (A.2.4) becomes:

$$\int_V \nabla^2 G\left(\vec{r}, \vec{r}'\right) dV = \int_S (\nabla G) \cdot d\vec{A} = 4\pi R^2 \left.\frac{dG}{dr}\right|_{r=R} \tag{A.2.5}$$

This yields

$$\frac{dG}{dr} = \frac{1}{4\pi r^2} \qquad \longrightarrow \qquad G(r) = -\frac{1}{4\pi r} + \text{const.} \tag{A.2.6}$$

The boundary condition that G vanishes at infinity fixes the constant to be zero and we have

$$G\left(\vec{r}, \vec{r}'\right) = -\frac{1}{4\pi \left|\vec{r} - \vec{r}'\right|} \tag{A.2.7}$$

Thus, the solution to (A.2.1) is

$$u(\vec{r}) = -\frac{1}{4\pi}\int \frac{\rho(\vec{r}')}{|\vec{r}-\vec{r}'|}d^3\vec{r}' \tag{A.2.8}$$

We can now use this general solution to solve our Poisson's equation for the potential (A.1.17), which gives us:

$$\Phi(\vec{r},t) = -\mathcal{G}m\int \frac{|\psi(\vec{r}',t)|^2}{|\vec{r}-\vec{r}'|}d^3\vec{r}' + \frac{\Lambda c^2}{4\pi}\int \frac{1}{|\vec{r}-\vec{r}'|}d^3\vec{r}' \tag{A.2.9}$$

Appendix B

Analytic Time Evolution of the Gaussian Wave Function

The eigenfunction of the Hamiltonian of a free particle moving in three-dimensional space is given by:

$$\phi_{\vec{k}}(\vec{r}) = \frac{1}{(2\pi)^{3/2}} e^{i\vec{k}\cdot\vec{r}} \tag{B.0.1}$$

An arbitrary wave function $\psi(\vec{r})$ can be expressed in terms of the eigenfunctions as follows:

$$\psi(\vec{r}) = \int_{-\infty}^{\infty} \tilde{\psi}(\vec{k})\phi_{\vec{k}}(\vec{r})\mathrm{d}^3\vec{k} \tag{B.0.2}$$

where

$$\tilde{\psi}(\vec{k}) = \int_{-\infty}^{\infty} \phi^*_{\vec{k}}(\vec{r})\psi(\vec{r})\mathrm{d}^3\vec{r} \tag{B.0.3}$$

In the case of spherical symmetry and substituting the expression for $\phi_{\vec{k}}(\vec{r})$ and $\phi^*_k(\vec{r})$, equation (B.0.2) and (B.0.3) become:

$$\psi(r) = \frac{1}{2\pi^2 r} \int_0^{\infty} k \sin(kr)\tilde{\psi}(k)\mathrm{d}k \tag{B.0.4}$$

$$\tilde{\psi}(k) = \frac{4\pi}{k} \int_0^{\infty} r \sin(kr)\psi(r)\mathrm{d}r \tag{B.0.5}$$

Substituting our initial wave function (1.4.1) into (B.0.5) and integrating by parts, we get:

$$\tilde{\psi}(k) = \frac{4\pi}{k}\left(\frac{\alpha}{\pi}\right)^{\frac{3}{4}} \int_0^\infty r\sin(kr)e^{-\alpha r^2/2}\mathrm{d}r = 2\sqrt{2}\left(\frac{\pi}{\alpha}\right)^{\frac{3}{4}} e^{-k^2/2\alpha} \tag{B.0.6}$$

Using (B.0.6) and (B.0.4), we can obtain the expressioin for $\psi(r,t)$ as follows:

$$\psi(r,t) = \frac{1}{2\pi^2 r}\int_0^\infty k\sin(kr)\tilde{\psi}(k)e^{-\frac{E}{\hbar}t}\mathrm{d}k \tag{B.0.7}$$

$$= \frac{\sqrt{2}}{\pi^2 r}\left(\frac{\pi}{\alpha}\right)^{\frac{3}{4}} \int_0^\infty k\sin(kr)\exp\left[-\left(\frac{m+i\alpha\hbar t}{2\alpha m}\right)k^2\right]\mathrm{d}k \tag{B.0.8}$$

where we have used $E = \hbar^2k^2/(2m)$. Integrating by parts gives us:

$$\psi(r,t) = (\pi\alpha)^{-\frac{3}{4}}\left(\frac{\alpha m}{m+i\alpha\hbar t}\right)^{\frac{3}{2}}\exp\left(-\frac{\alpha m}{2(m+i\alpha\hbar t)}r^2\right) \tag{B.0.9}$$

Appendix C

Expanding the Inverse Distance

Consider the following inverse distance between two vectors:

$$\frac{1}{|\vec{r}-\vec{r}'|} = \left(r^2 + r'^2 - 2rr'\cos\gamma\right)^{-\frac{1}{2}} = \frac{1}{r}\left[1 + \left(\frac{r'}{r}\right)^2 - 2\frac{r'}{r}\cos\gamma\right]^{-\frac{1}{2}} \tag{C.0.1}$$

where r and r' are the magnitude of the vectors $\vec{r}$ and $\vec{r}'$ respectively and γ is the angle between $\vec{r}$ and $\vec{r}'$. Let $\epsilon = \left(\frac{r'}{r}\right)\left(\frac{r'}{r} - 2\cos\gamma\right)$. For $\epsilon \ll 1$, we can perform the binomial expansion as follows:

$$\begin{aligned}
\frac{1}{r}(1+\epsilon)^{-1/2} =& \frac{1}{r}\left[1 - \frac{1}{2}\epsilon + \frac{3}{8}\epsilon^2 - \frac{5}{16}\epsilon^3 + \cdots\right] \\
=& \frac{1}{r}\left[1 - \frac{1}{2}\left(\frac{r'}{r}\right)\left(\frac{r'}{r} - 2\cos\gamma\right) + \frac{3}{8}\left(\frac{r'}{r}\right)^2\left(\frac{r'}{r} - 2\cos\gamma\right)^2 + \cdots\right] \\
=& \frac{1}{r}\left[1 + \left(\frac{r'}{r}\right)\cos\gamma + \left(\frac{r'}{r}\right)^2\frac{3\cos^2\gamma - 1}{2} + \cdots\right]
\end{aligned}$$

Thus, (C.0.1) can be expressed in terms of the Legendre polynomials:

$$\frac{1}{|\vec{r}-\vec{r}'|} = \frac{1}{r}\sum_{l=0}^{\infty}\left(\frac{r'}{r}\right)^l P_l(\cos\gamma) \qquad \text{for} \qquad r' < r \tag{C.0.2}$$

It is convenient to introduce the notations: $r_< = \min\{r, r'\}$ and $r_> = \max\{r, r'\}$. Thus, (C.0.2) becomes:

$$\frac{1}{|\vec{r}-\vec{r}'|} = \frac{1}{r_>}\sum_{l=0}^{\infty}\left(\frac{r_<}{r_>}\right)^l P_l(\cos\gamma) \tag{C.0.3}$$

The addition theorem of spherical harmonics is given by:

$$P_l(\cos\gamma) = \frac{4\pi}{2l+1}\sum_{m=-l}^{l} Y_l^m(\theta,\phi)Y_l^m(\theta',\phi')^* \tag{C.0.4}$$

Here, θ and ϕ represent the anglular coordinates of $\vec{r}$; θ' and ϕ' represent the anglular coordinates of $\vec{r}'$; and γ is the angle between $\vec{r}$ and $\vec{r}'$.The derivation of the addition theorem of spherical harmonics can be found in [13]. Substituting (C.0.4) into (C.0.3) gives:

$$\frac{1}{|\vec{r}-\vec{r}'|} = 4\pi\sum_{l=0}^{\infty}\frac{1}{2l+1}\frac{r_<^l}{r_>^{l+1}}\sum_{m=-l}^{l} Y_l^m(\theta,\phi)Y_l^m(\theta',\phi')^* \tag{C.0.5}$$

With (C.0.5) in mind, we can solve the following integral in a relatively simple way.

$$\begin{aligned}\int\frac{d\Omega'}{|\vec{r}-\vec{r}'|} &= 4\pi\sum_{l=0}^{\infty}\frac{1}{2l+1}\frac{r_<^l}{r_>^{l+1}}\sum_{m=-l}^{l} Y_l^m(\theta,\phi)\int Y_l^m(\theta',\phi')^*d\Omega' \\ &\mid \quad \int Y_l^m(\theta',\phi')^*d\Omega' = \sqrt{4\pi}\int Y_0^0(\theta',\phi')Y_l^m(\theta',\phi')^*d\Omega' \\ &\mid \text{ Spherical Harmonics are orthonormal, so} \\ &\mid \quad \int Y_l^m(\theta',\phi')^*d\Omega' = \sqrt{4\pi}\delta_{l0}\delta_{m0} \\ &= \frac{4\pi}{r_>}Y_0^0(\theta,\phi)\sqrt{4\pi}\end{aligned} \tag{C.0.6}$$

Therefore, we have

$$\int\frac{d\Omega'}{|\vec{r}-\vec{r}'|} = \begin{cases}\dfrac{4\pi}{r} & \text{if } r'<r \\ \\ \dfrac{4\pi}{r'} & \text{if } r'>r\end{cases} \tag{C.0.7}$$

Hence, the integral describing our potential can be simplified into the following form in the case of a spherically symmetric wave function:

$$\begin{aligned}\Phi(r,t) &= -\mathcal{G}m\int_0^\infty |\psi(r',t)|^2 r'^2 \int \frac{d\Omega}{|\vec{r}-\vec{r'}|}dr' + \frac{\Lambda c^2}{4\pi}\int_0^\infty r'^2 \int \frac{d\Omega}{|\vec{r}-\vec{r'}|}dr' \\ &= -4\pi\mathcal{G}m\left(\frac{1}{r}\int_0^r |\psi(r',t)|^2 r'^2 dr' + \int_r^\infty |\psi(r',t)|^2 r' dr'\right) \\ &\quad + \Lambda c^2\left(\frac{1}{r}\int_0^r r'^2 dr' + \int_r^\infty r' dr'\right) \end{aligned} \tag{C.0.8}$$

Appendix D

Numerics Written in MATLAB

Here we present the numerics used to solve the SNΛ equation written in MATLAB. This numerics can also be used to recover the solutions to SN equation by setting the parameter Λ to be zero.

```
tic
clear
clc

%Parameters
alpha = 1.78E-4;              %Gaussian parameter
N = 370;                      %Number of position-step
Nt = 12000;                   %Number of time-step
j = linspace(0,8E2,N)';       %Position range
dr = j(2) - j(1);             %Size of position-step
n = linspace(0,1.1E18,Nt);    %Time range
dt = n(2) - n(1);             %Size of time-step

%Constants
G = 6.674E-11;              %Gravitational constant (m^3kg^-1s^-2)
hbar = 1.0546E-34;          %Planck Constant (Joule.second)
m = 5E-20;                  %mass of particle (kg)
lambda = 1.36E-52;          %Cosmological Constant (m^-2)
c = 3E8;                    %Speed of light (m/s)
R = dt/(dr^2);
K = 1i*hbar/(8*m);
```

```
22 P = 1i*dt/(2*hbar);
23
24 %Diagonal Vector
25 DV = zeros(N,1);
26
27 %Superdiagonal Vector
28 SuperDV = zeros(N,1);
29 for i = 2:N
30     SuperDV(i) = -K*R*(1-1/i);
31 end
32
33 %Subdiagonal Vector
34 SubDV = zeros(N,1);
35 SubDV(1) = -6*K*R;
36 for i = 2:N-1
37     SubDV(i) = -K*R*(1+1/i);
38 end
39
40 %Initial Wavefunction
41 Psi = zeros(N,Nt);
42 for i = 1:N
43     Psi(i,1) = (alpha/pi)^(3/4)*exp(-alpha*(j(i)^2)/2);
44 end
45
46 B = zeros(N,1);
47 D = zeros(N,1);
48 X = zeros(N,Nt);
49 V = zeros(N,Nt);     %Potential matrix
50
51 for k = 1:Nt-1
52     %Potential
53     I1 = 0;
54     I2 = 0;
55     I3 = 0;
56     I4 = 0;
57     for i = 0:N-1
```

```
58          if i == 0
59              I1 = 0;
60              I2 = sum(Psi(1:N,k).*conj(Psi(1:N,k)).*(0:N-1)');
61              I3 = 0;
62              I4 = sum(j(1:N));
63              V(1,k) = -4*pi*G*(m*dr)^2*I2+lambda*m*(dr)^2*c^2*I4
                    ;
64          else
65              I1 = sum(Psi(1:i,k).*conj(Psi(1:i,k)).*(0:i-1).^2)
                    ;
66              I2 = sum(Psi(i+1:N,k).*conj(Psi(i+1:N,k)).*(i:N-1)
                    ');
67              I3 = sum((j(1:i)).^2);
68              I4 = sum(j(i+1:N));
69              V(i+1,k) = -4*pi*G*(m*dr)^2*((1/i)*I1+I2)+lambda*m*
                    c^2*(((1/i)*I3)+((dr)*I4));
70          end
71      end
72
73      %Diagonal Vector
74      DV(1) = 0.5*(1+P*V(1,k)+12*K*R);
75      DV(2:N) = 0.5*(1+P*V(2:N,k)+2*K*R);
76
77      B(1) = DV(1);
78      D(1) = Psi(1,k);
79      for i = 2:N
80          B(i) = DV(i)-SuperDV(i)*SubDV(i-1)/B(i-1);
81          D(i) = Psi(i,k)-SuperDV(i)*D(i-1)/B(i-1);
82      end
83      X(N,k) = D(N)/B(N);
84      for i = N-1:-1:1
85          X(i,k) = (D(i)-SubDV(i)*X(i+1,k))/B(i);
86      end
87      Psi(:,k+1) = X(:,k)-Psi(:,k);
88  end
89
```

```
90 %Plot Wavefunction
91 figure
92 plot(j,Psi(:,1).*conj(Psi(:,1)).*j(:).^2);
93 hold on
94 plot(j,Psi(:,4000).*conj(Psi(:,4000)).*j(:).^2);
95 plot(j,Psi(:,8000).*conj(Psi(:,8000)).*j(:).^2);
96 plot(j,Psi(:,12000).*conj(Psi(:,12000)).*j(:).^2);
97 title('Numerical SN\Lambda Plot');
98 xlabel('r(m)');
99 ylabel('|\psi|^2r^2');
100 legend('t = 1', 't = 4000', 't = 8000','t = 12000');
101
102 toc
```

Bibliography

[1] F. Károlyházy. *Gravitation and Quantum Mechanics of Macroscopic Objects*, Nuovo Cim, A 42, 390 (1966).

[2] L. Diósi. *Gravitation and Quantum-Mechanical Localization of Macro-Objects*, Phys. Lett. A, 105:199-202 (1984).

[3] R. Penrose, *On Gravity's Role in Quantum State Reduction*, Gen. Rel. Grav., 28 (5): 581–600 (1996).

[4] A. Bassi, K. Lochan, S. Satin, T.P. Singh, H. Ulbritch, *Models of Wave Function Collapse, Underlying Theories and Experimental Tests*, Rev. Mod. Phys. 85, 471 (2013).

[5] C. Møller. *Les Theories Relativistes de la Gravitation*, CNRS, Paris (1962).

[6] L. Rosenfeld. Nucl. Phys. 40, 353 (1963).

[7] A. G. Riess et al. *Observational Evidence from Supernovae for an Accelerating Universe and Cosmological Constant*, Astron. J. 116, 1009 (1998).

[8] J. P. Ostriker, P. J. Steinhardt. *Cosmological Concordance*, astro-ph/9505066. 1995.

[9] T. W. Kibble and S. Randjbar-Daemi. *Non-Linear Coupling of Quantum Theory and Classical Gravity*, J. Phys. A, 13:141-148 (1980).

[10] C. Beck. *Axiomatic Approach to the Cosmological Constant*, Physica. A, 388:3384-3390 (2008).

[11] J. B. Hartle. Gravity: *An Introduction to Einstein's General Relativity.* Pearson Education, Inc. (2003).

[12] P. J. Salzman. *Investigation of the Time-Dependent Schrödinger-Newton Equation*, PhD Thesis, University of California Davis (2005).

[13] G. B. Arfken, H. J. Weber, and F. E. Harris. *Mathematical Methods for Physicists*, 7th edition. Academic Press, Elsevier, Inc., Waltham, MA (2013).

[14] W. H. Press, S. A. Teukolsky, W. T. Vetterling, and B. P. Flannery. *Numerical Recipes in C: The Art of Scientific Computing*, Cambridge University Press, 2nd edition (1995).

[15] D. Giulini and A. Großardt. *Gravitaional Induced Inhibitions of Dispersion According to the Schrödinger-Newton Equation*, Class. Quant. Grav., 28 (2011).

[16] S. Carlip. *Is Quantum Gravity Necessary?*, Class. and Quant. Grav., 25(15):107-144 (2008).

[17] S. Bhattacharya, K. F. Dialektopoulos, A. E. Romano, C. Skordis and T. N. Tomaras, The Maximum Sizes of Large Scale Structures in Alternative Theories of Gravity, arXiv:1611.05055 [astro-ph.CO].